INFLUENCE OF DYNAMIC ABSORBERS ON A THREE DIMENSIONAL TRUSS

by

Denis Branthonne

Ingénieur diplômé de L'Ecole Nationale Superieure des Techniques Avancées

Submitted to the Department of Ocean Engineering
in partial fulfillment of the Requirements
for the Degrees of

MASTER OF SCIENCE
IN OCEAN ENGINEERING

at the
MASSACHUSETTS INSTITUTE OF TECHNOLOGY

August, 1994.

Author ____
_____
Department of Ocean Engineering
August, 1994

Certified by
_____
Professor Ira Dyer
Thesis Supervisor

Accepted by
_____
Professor A. Douglas Carmichael
Chairman, Department Graduate Committee

INFLUENCE OF DYNAMIC ABSORBERS ON A THREE DIMENSIONAL TRUSS

by

Denis Branthonne

Submitted to the department of Ocean Engineering on August 1, 1994
in partial fulfillment of the requirements for the degree of
Master of Science in Ocean Engineering

Abstract

The objective of this thesis is to explore experimentally the effects of adding dynamic absorbers to a three dimensional truss and to design analytical models which predi the phenomena of attenuation.

The structure being tested is a $4.7 \times 0.84 \times 0.8$ m truss comprised of cells made of aluminium rods and connected in series. 110 dynamic absorbers with a longitudinal and flexural resonant frequency of 450 Hz and a torsional resonant frequency of 330 Hz are mounted on the rods in the center cell to achieve a local mass ratio of 3. The truss is excited at one end with white noise to measure the spatial attenuation averaged on octave bands as a function of axial distance over the frequency range from 125 Hz to 8 kHz. The data are compared to the spatial attenuation for the undamped structure. The differences determine the effect of the dynamic absorbers. The overall shape of the differential curves of attenuation versus axial distance is a step function, with the step located in the dynamic absorbers attachment area.

Assuming the equi-partition of energy between the different wave types and using the classical theory of attenuation of waves propagating on a semi-infinite rod loaded with a continuous layer of dynamic absorbers, one predicts stronger attenuation than experimental data at low frequencies (especially in the 500 Hz octave band). The assumption of equi-partition of energy proves to be incorrect and the applicability of the semi-infinite model is questioned. Subsequently, a new theory is derived and validated by experiment to describe the attenuation of waves on finite rods loaded with a layer of dynamic absorbers. At low frequencies, this model achieves a better estimation of the axial attenuation along the truss. At high frequencies, the difference of impedance between the attached masses and the unloaded rod results in the reflection of waves and explains the high level of attenuation observed on experimental curves.

Thesis Supervisor: Dr. Ira Dyer

Title: Professor

Acknowledgments

First, I would like to thank Professor Ira Dyer for his guidance in experimentation and interpretation of results.

I am grateful to Dr. Joe Bondaryk for his support, encouragement and thought provoking discussions. His meticulous advice greatly helped me to write this thesis.

I would like to thank Dr. Yueping Guo for his contribution to analytical models, Matthew Conti for his help in the understanding of previous studies dealing with dynamic absorbers and Tarun Kapoor for his programming support and his excellent coffee.

I would like to thank my officemates and my colleagues in the Acoustics and Vibrations Laboratory for their help and support.

Successful experimentation would not have been possible without the assistance of Marcus Heath.

And a special thank to Gilles Cochevelou who helped me to apply at MIT. His advice and the financial support of DCN Cherbourg is greatly appreciated.

Table of Contents

List of Figures

List of Tables

List of Symbols

A_f	Attenuation of longitudinal waves in dB
A_L	Attenuation of longitudinal waves in dB
A_T	Attenuation of longitudinal waves in dB
a	accelerance
β	mass ratio
c_f	flexural wave speed
c_L	longitudinal wave speed
c_T	torsional wave speed
d	spacing of the dynamic absorbers
E	Young's modulus
e	base of the Naperian log, e = 2.71828.....
f	frequency
f_{cr}	critical frequency
γ_f	flexural loss factor of the dynamic absorber
γ_L	longitudinal loss factor of the dynamic absorber
γ_T	torsional loss factor of the dynamic absorber
I	moment of inertia of the rod
I_f	flexural wave energy
I_L	longitudinal wave energy
I_T	torsional wave energy
i	square root of -1
k_f	normal stiffness per unit area of the layer
k_L	longitudinal stiffness per unit area of the layer
k_T	torsional stiffness per unit area of the layer
K_f	complex flexural wavenumber of the loaded rod
K_{fi}	imaginary part of K_f
K_{fr}	real part of K_f
K_L	longitudinal wavenumber of the loaded rod
K_T	torsionalwavenumber of the loaded rod
κ_f	flexural wavenumber of the unloaded rod

κ_T	torsional wavenumber of the unloaded rod
κ_L	longitudinal wavenumber of the unloaded rod
M	mass per unit area of the rod
m	mass per unit area of the layer
R_f	normal resistance per unit area of the layer
R_L	longitudinal resistance per unit area of the layer
R_T	torsional resistance per unit area of the laye
r_{inner}	inner radius of the attached mass
r_{outer}	inner radius of the attached mass
r_1	outer radius of the rod
r_2	inner radius of the attached mass = r_{inner}
χ_{abs}	radius of giration of the attached mass
$\mathcal{R}$	reflection coefficient
S	area of the rod
t	time
τ	transmission coefficient
θ_1	angular displacement of the rod
θ_2	angular displacement of the attached mass
u_1	normal displacement of the rod
u_2	normal displacement of the attached mass
v_1	longitudinal displacement of the rod
v_2	longitudinal displacement of the attached mass
ω	radian frequency
ω_{0f}	flexural resonance frequency of the dynamic absorber
ω_{0L}	longitudinal resonance frequency of the dynamic absorber
ω_{0T}	torsional resonance frequency of the dynamic absorber
x	axial distance along the rod
Z_1	impedance of the rod

1 Introduction

The importance of the control of vibrational energy in truss-like structures has been driven by recent developments in submarine design. The idea for mounting submarine machinery on a cradle structure first emerged in France, in the beginning of the 1980's. Studies were conducted by the Délégation Générale de l'Armement. The design of the French nuclear submarine type "Le Triomphant" is based on this concept. The progression towards this design was driven by the requirement of using modularity in fabrication and assembly. The architecture of a conventional architecture and a typical cradle structure is presented in fig 1.1.

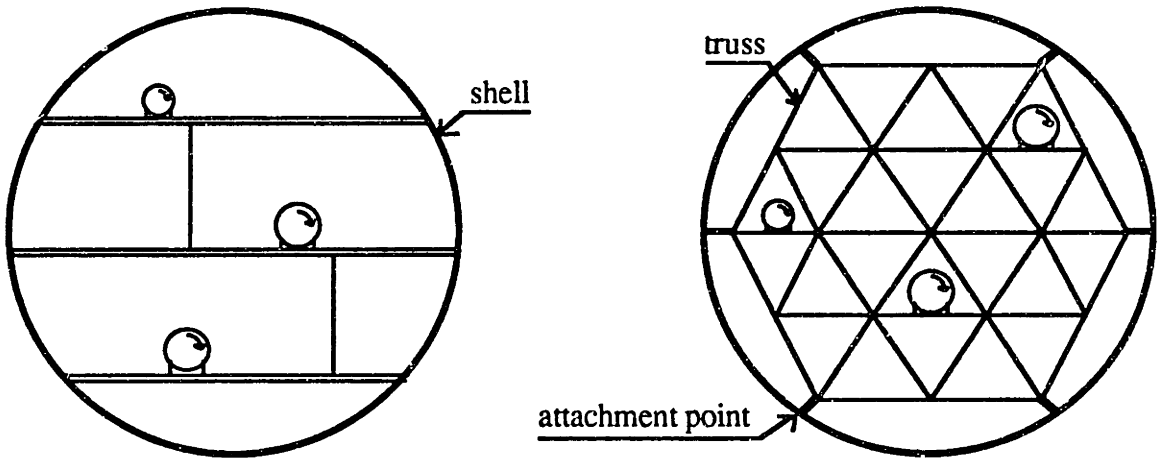

Conventional architecture Cradle structure architecture

Figure 1.1: Schematic of a submarine cross-section showing conventional architecture and cradle structure architecture.

In the conventional architecture, the machinery is mounted on decks, which are in turn resiliently mounted almost continuously to the shell. In the new architecture, the cradle is the truss structure which supports the machinery. The cradle is located at the back of the submarine and is connected to the shell at a limited number of attachment points. The use of

a cradle structure provides separation between the interior structural dynamics and the hull dynamics. As a consequence, different mechanisms can be employed to isolate the internal sources of noise from the hull to minimize the underwater noise signature of the entire vessel. The propagation of unwanted vibration can be reduced either at (a) the attachment points or (b) within the truss.

a. Since the shell is a pressure vessel, stable against collapse and buckling modes, the submarine internals need not contribute to the global strength of the outer shell. Therefore, the cradle can be isolated from the outer shell by isolation mounts at a limited number of attachment points. The design of these attachment points allows control of low frequency radiation and shock.

b. The truss provides a tortuous path through which vibratory energy must travel before it reaches the shell. Specific design of the truss components or added damping can then be applied to reduce vibrations before they reach the attachment points and the hull.

1.1 Previous Research

MIT's research on machinery cradle damping began in early 1993. The objective of this program is to understand the dynamics of complicated truss-like structures with localized or distributed damping. A three dimensional truss was designed and built for laboratory testing. Marcus R. A. Heath has explored the dynamics of this truss to determine the inherent type and degree of damping [1]. He has shown that strut radiation is the main mechanism of attenuation for all frequencies above a critical value. Other mechanisms of attenuation such as radiation from joints, losses in the interface between components and losses to ground through the supports, are negligible compared to the attenuation due to scattering and strut radiation.

Many treatments can be used to achieve efficient damping of a truss structure. For example, filling the hollow truss members with visco-elastic particulates, polyethylene beads or sand achieve high frequency attenuation. This type of treatment has been studied by the laboratories of the Délégation Générale de l'Armement and is currently being studied at the Carderock Naval Surface Warfare Center and at MIT by Mark Hayner. Unwanted vibratory energy can also be controlled by the application of uniformly distributed damping layers placed on the truss members that absorb the waves via transfer of vibratory energy to dissipating elements in the layer; this technology is very well developed and is often used .

Another form of control is the use of a layer of dynamic absorbers [2]. Waves are attenuated by a distribution of masses resiliently mounted to the structure. The dynamic absorber layer inhibits the wave by presenting a very high wave impedance over a region which is large compared to the wavelength of propagating waves.

1.2 Objectives

The use of dynamic absorbers applied in a local region of the truss has been identified by the MIT research team as a potential treatment for especially noisy source regions or especially sensitive mounting areas. The objective of this thesis is to explore the effects of adding dynamic absorbers to the MIT truss and design analytical models to predict the phenomena of attenuation.

Dynamic absorbers are added on a section in the middle of the truss so that no wave can propagate from one part to the other without going through a treated rod. The attenuation versus axial distance is measured along the truss. These data are compared with the attenuation for the unloaded truss, showing the effect of the added dynamic absorbers.

Previous studies conducted at MIT focus on the attenuation of flexural and longitudinal waves on semi-infinite rods loaded with a layer of dynamic absorbers [3] [4]. In this study, the treated rods involved in the truss are finite. The three kinds of waves present in the truss, flexural, longitudinal and torsional, are studied analytically. A new model taking into account finite boundary conditions is built and validated by experiment. The aim is to understand the mechanisms of wave attenuation due to the addition of dynamic absorbers by comparing analytical predictions to measured axial attenuation.

1.3 Approach

Analytical models dealing with the attenuation of flexural and longitudinal waves on semi-infinite rods are recalled in Chapter 2. A model of attenuation for torsional waves is derived from the longitudinal case.

In Chapter 3, the design and building of different types of dynamic absorbers is described. Single test experiments define their flexural and longitudinal resonance frequencies; the torsional resonance frequency is calculated. A specific design is chosen to insure that the mass ratio is high enough to influence the truss structure and that the resonance frequencies allow a satisfactory frequency range of efficiency.

Chapter 4 deals with the measurement on the $4.7 \times 0.84 \times 0.8$ m truss of the axial attenuation due to the addition of dynamic absorbers. A large number of absorbers is built and mounted on the truss. A section in the middle of the truss is treated so that no wave can propagate from one end to the other without going through a treated rod. The truss is excited at one end by random noise on octave bands frequencies from 125 Hz to 8 kHz. The spatial attenuation as a function of axial distance is determined by measuring the acceleration at the joints. The data are compared to the spatial attenuation for the undamped structure. The difference is plotted and determines the effect of the dynamic absorbers. The overall shape of the experimental curves of attenuation versus axial distance is a step function, with the step located in the dynamic absorbers attachment area. The step is dramatic between 250 Hz and 4 kHz, with a maximum at 2 kHz.

Experimental curves and expectations due to theoretical models are compared and discussed in Chapter 5. Assuming the equi-partition of energy and using the analytical models recalled in Chapter 2, one predicts a stronger attenuation between 300 Hz and 1 kHz, and minor effects above. The assumption of equi-partition of energy proves to be incorrect. The equi-partition of acceleration is a more realistic assumption. Also, the analytical models are designed for semi-infinite rods and are not valid for high frequencies. Therefore, a new analytical model is proposed to take into account the finite boundary conditions of the rods involved in the truss. An experiment is conducted to validate this theory. A rod located in the treated area of the truss is populated with accelerometers. Excitation is provided at one end of the rod. The attenuation of flexural waves is measured and plotted. This experiment shows the validity of the new model and also proves that the attenuation of flexural waves is actually taking place in the truss but with a smaller amplitude than the previous predictions. This confirms the experimental curves plotted in Chapter 4. Mechanisms of attenuation involved at high frequencies are explored in the last section of Chapter 5.

Chapter 6 summarizes the major results of this thesis and provides suggestions for future research. This study shows that the use of dynamic absorbers applied in a local region of a truss is a potential treatment for especially noisy source regions. The comparison between experiment and analytical predictions proves that the assumption of equi-partition of energy in the truss is not valid at low frequencies. Future work should focus on the determination of the partitioning of energy in the truss and should also define the behavior of dynamic absorbers at frequencies for which the continuity assumption is no longer valid.

2 Analytical Models for the Attenuation of Rod Waves by a Layer of Dynamic Absorbers

A layer of dynamic absorbers mounted on a semi-infinite rod can attenuate the amplitude of propagating flexural, longitudinal and torsional waves. This chapter describes the mechanisms involved and provides analytical models for them. The flexural and longitudinal equations are found in previous studies [2] [3] [4] [5]. By using some assumptions for the resilient material, it is possible to derive the torsional attenuation from the longitudinal case.

2.1 Attenuation of Flexural Waves due to a Layer of Dynamic Absorbers

Consider a semi-infinite circular rod with regularly spaced, resiliently mounted discs acting as a dynamic absorber layer. The model is symmetric with possible structural imperfections ignored. Waves are one-dimensional and right traveling. A schematic is depicted in Fig 2.1 below.

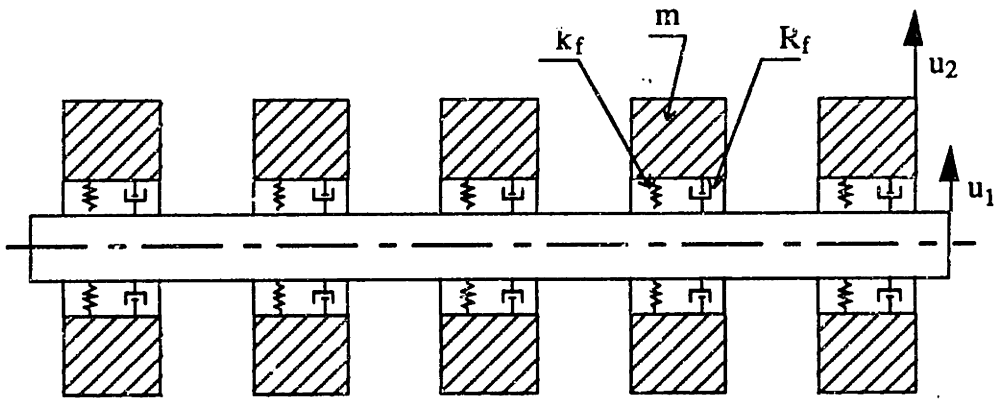

Figure 2.1: Transverse view of a semi-infinite circular rod with a dynamic absorber layer

The spacing of the dynamic absorbers is small compared to a wavelength so that continuity of the layer can be assumed. The coupled equations of motion are:

$$EI\nabla^4 u_1 + M\frac{\partial^2 u_1}{\partial t^2} + R_f\frac{\partial}{\partial t}(u_1-u_2) + k_f(u_1-u_2) = 0 \qquad (2.1)$$

$$m\frac{\partial^2 u_2}{\partial t^2} + R_f\frac{\partial}{\partial t}(u_2-u_1) + k_f(u_2-u_1) = 0 \qquad (2.2)$$

where E is the Young's Modulus; I the area moment of inertia of the rod; M the mass per unit area of the rod; R_f, k_f, and m the per unit area resistance, stiffness, and mass respectively of the layer; u_1 and u_2 the normal displacement of the rod and the attached mass respectively, as shown in Fig 2.1.

Equations assume that the shear deformation and rotational energy contributions are negligible. Additionally, the resilient layer is considered massless and thin compared to a wavelength. Losses associated with the resilient layer are considered dominant, and losses in the structural layers are ignored.

We now seek solutions to Eq. (2.1) and (2.2) of the form

$$u_1 = \exp(iK_f x - i\omega t) \qquad (2.3)$$

where K_f is the flexural wavenumber (2pi / wavelength) and ω the radian frequency. With some manipulation we can find that one-dimensional harmonic waves, described by Eq. (2.3), exist if

$$K_f^4 = \kappa_f^4\left[1+\beta\frac{\gamma_f + i\omega_{0f}^2/\omega^2}{\gamma_f + i(\omega_{0f}^2/\omega^2 - 1)}\right] \qquad (2.4)$$

where $\beta = \frac{m}{M}$ the mass ratio

$\gamma_f = \frac{R_f}{\omega m}$ the loss factor of the dynamic absorbers

$\omega_{0f}^2 = \frac{k_f}{m}$ the square of the dynamic absorber flexural resonance frequency

$\kappa_f^4 = \omega^2\frac{M}{EI}$ the fourth power of the flexural wavenumber without the layer

The wavenumber has interesting behavior. For the simple case $\gamma_f = 0$ (no damping),

$$K_f^4 = \kappa_f^4\left[1+\beta/(1-\omega^2/\omega_{0f}^2)\right] \qquad (2.5)$$

we can see that K_f has an imaginary part for frequencies defined by

$$1 < \omega/\omega_{\gamma f} < \sqrt{1+\beta} \tag{2.6}$$

since the fourth-power term in Eq. (2.5) then entails a root of a negative quantity. We can call the domain of Eq. (2.6) an attenuation band induced by the layer, since wherever the imaginary part of K_f ($=K_{fi}$) exists, the spatial dependence becomes $\exp(iK_{fi}x - K_{fr}x)$, where K_{fr} and K_{fi} are the real and imaginary parts of K_f respectively. Of course for any practical layer $\gamma > 0$, and the results in Eqs. (2.5) and (2.6) are not entirely applicable.

Without any approximation, the resulting flexural attenuation in dB per unit distance is

$$A_f = 20\log(e)K_{fi} = 8.686K_{fi} \quad \text{dB/unit of distance} \tag{2.7}$$

This attenuation is plotted in Fig 2.2 and 2.3 for different values of the mass ratio and the loss factor.

It appears that as the loss factor increases, the peak attenuation decreases and the band widens, more so towards the higher frequencies. Note also that as the mass ratio increases for fixed loss factor, the attenuation bandwidth increases, and the peak attenuation increases. Thus mass is doubly beneficial, but dissipation serves to increase bandwidth at the cost of reduced peak attenuation.

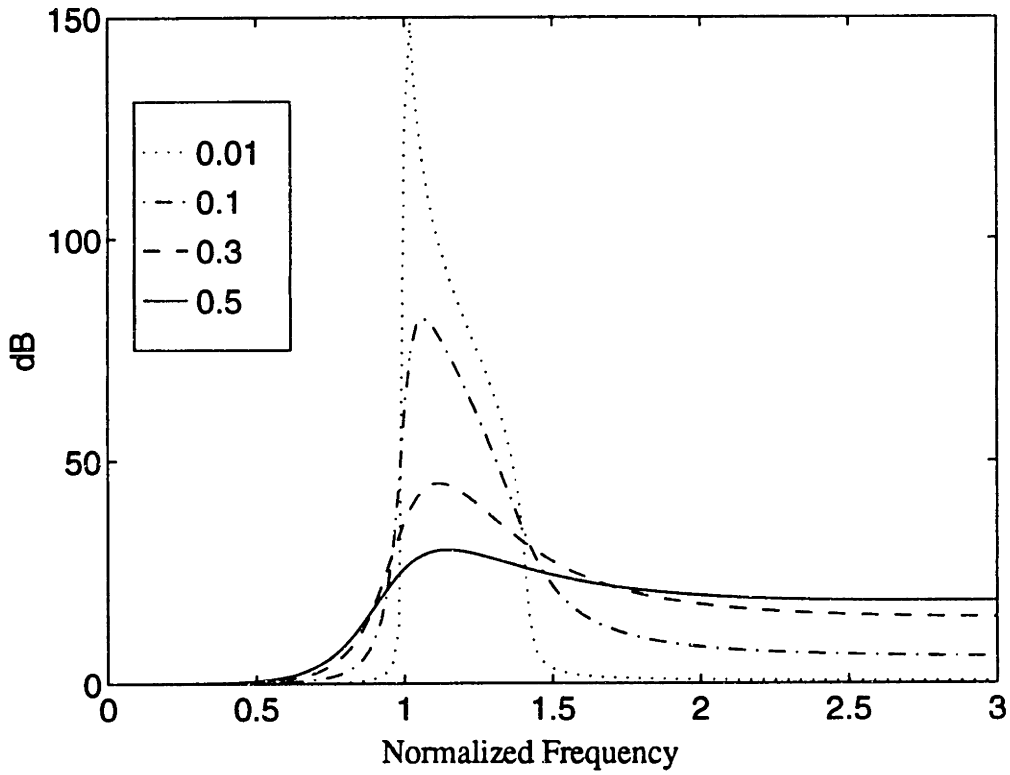

Figure 2.2: Predicted flexural attenuation per meter for β=1; the parameter is γ_f .

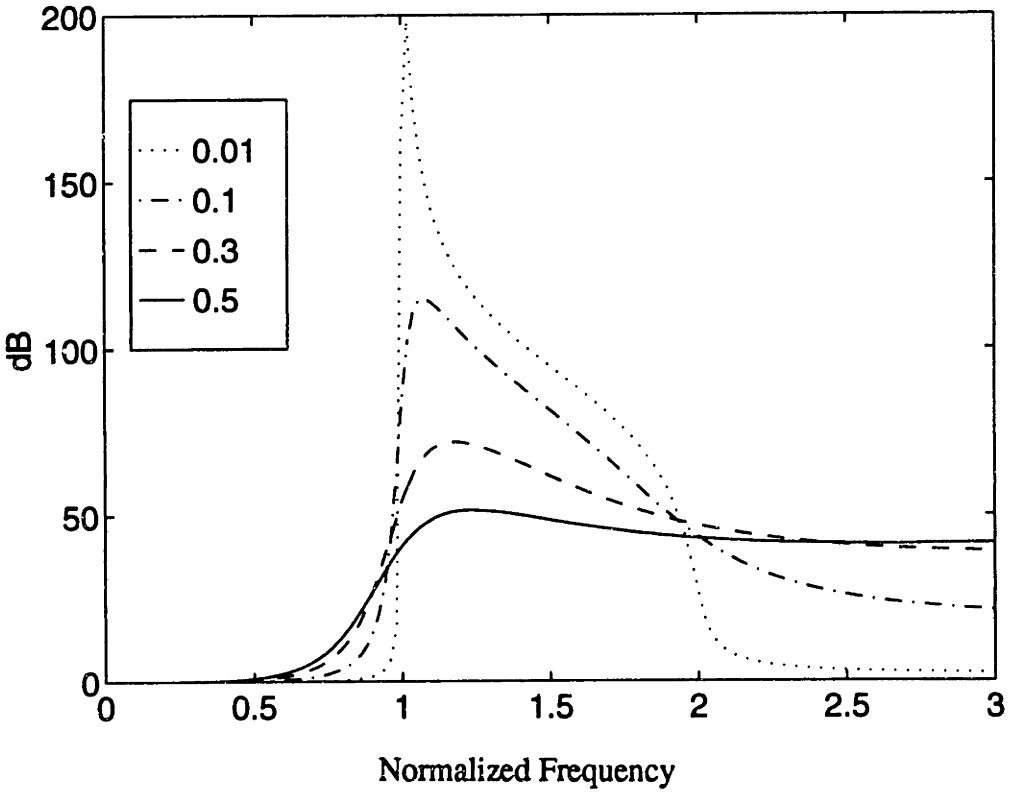

Figure 2.3: Predicted flexural attenuation per meter for β=3; the parameter is γ_f .

2.2 Attenuation of Longitudinal Waves due to a Layer of Dynamic absorbers

We consider the same rod with a layer of dynamic absorbers to understand the effect of dynamic absorbers on longitudinal waves.

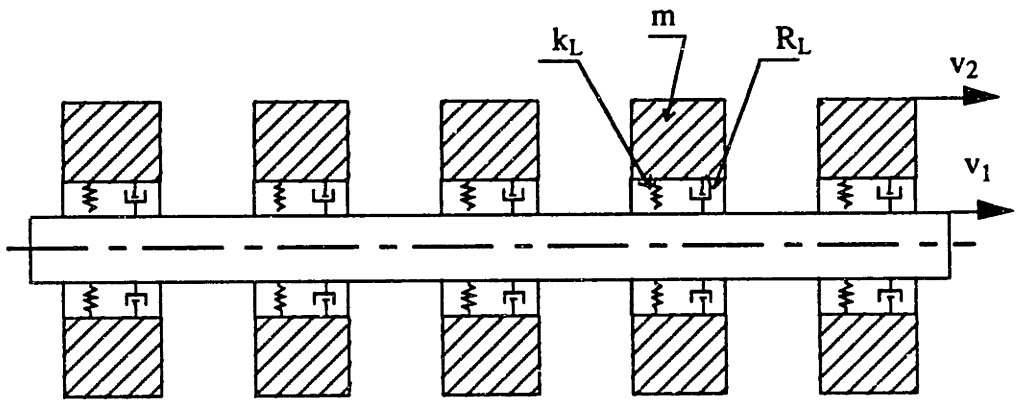

Figure 2.4: Transversal view of a semi-infinite circular rod with a dynamic absorber layer

The spacing of the dynamic absorbers is small compared to a longitudinal wavelength, so that continuity of the layer can be assumed. The coupled equations of motion are

$$-ES\frac{\partial^2 v_1}{\partial x^2} + M\frac{\partial^2 v_1}{\partial t^2} + R_L\frac{\partial}{\partial t}(v_1-v_2) + k_L(v_1-v_2) = 0 \tag{2.8}$$

$$m\frac{\partial^2 v_2}{\partial t^2} + R_L\frac{\partial}{\partial t}(v_2-v_1) + k_L(v_2-v_1) = 0 \tag{2.9}$$

where E and S are the modulus of elasticity and area of the rod; M the mass per unit area of the rod; R_L, k_L, and m the per unit area resistance, stiffness, and mass respectively of the layer; v_1 and v_2 the longitudinal displacement of the rod and the attached mass respectively, as show in Fig 2.4. To develop these equations, the same assumptions are made as in the flexural case. However, the values of the resistance R_L and stiffness k_L are different because the resilient material may have different stiffnesses and resistances when deflected in different directions.

We now seek solutions to Eq. (2.8) and (2.9) of the form

$$v_1 = \exp(K_L\, ix - i\omega t) \tag{2.10}$$

With some manipulation we find that harmonic waves exist if

$$K_L^2 = \kappa_L^2\left[1+\beta\,\frac{\gamma_L + i\omega_{0L}^2/\omega^2}{\gamma_L + i(\omega_{0L}^2/\omega^2 - 1)}\right] \tag{2.11}$$

where $\beta = \frac{m}{M}$ the mass ratio

$\gamma_L = \frac{R_L}{\omega m}$ the loss factor of the dynamic absorbers

$\omega_{0L}^2 = \frac{k_L}{m}$ the square of the dynamic absorber longitudinal resonance frequency

$\kappa_L = \frac{\omega}{c_L}$ the rod longitudinal wavenumber in the absence of the layer

and c_L is the longitudinal speed defined by $c_L = \sqrt{\frac{ES}{M}}$ (2.12)

Similarly, the resulting longitudinal attenuation in dB per unit distance is

$$A_L = 20\log(e)K_L i = 8.686K_L i \quad \text{dB/unit of distance} \tag{2.13}$$

The attenuation is plotted in fig 2.5 and 2.6 for different values of the mass ratio and the loss factor.

The behavior is the same as the flexural case. As the loss factor increases, the peak attenuation decreases and the band widens, more so towards the higher frequencies. And as the mass ratio increases for fixed loss factor, the attenuation bandwidth increases, and the peak attenuation increases.

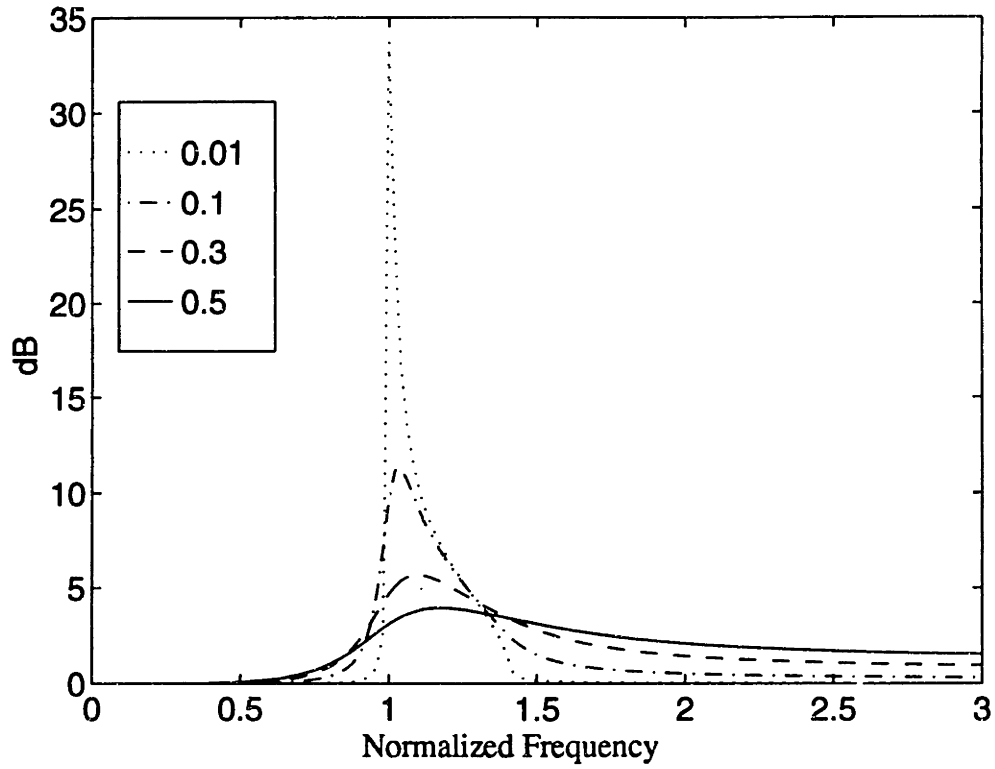

Figure 2.5: Predicted longitudinal attenuation per meter for β=1; the parameter is γ_L.

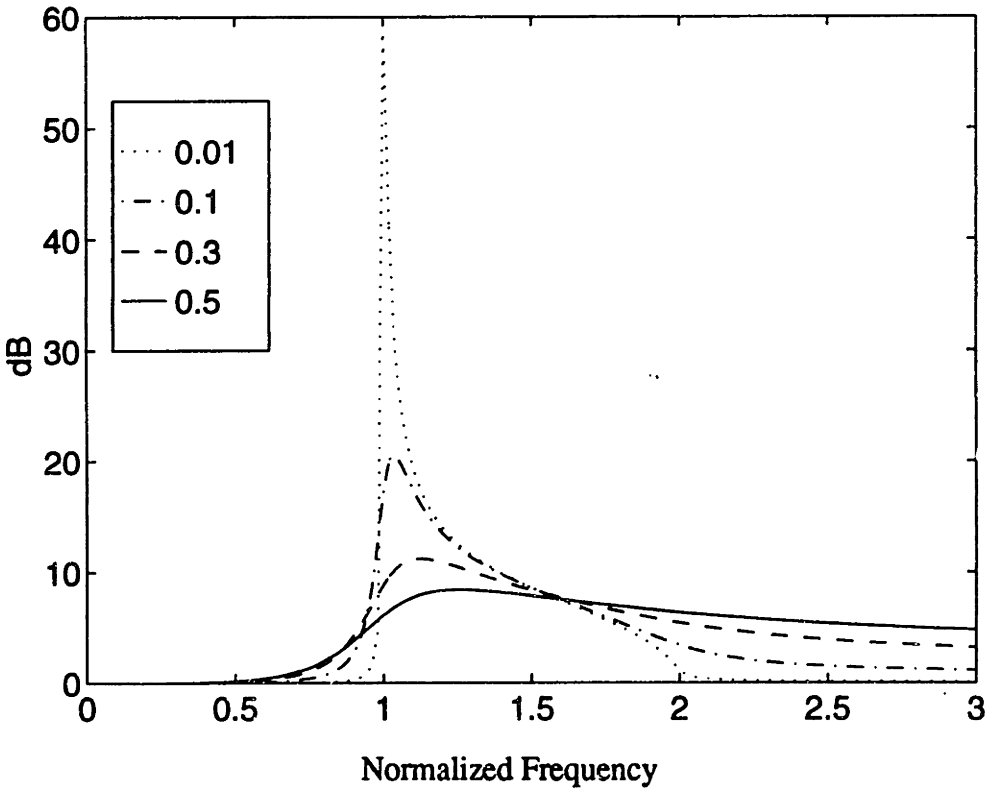

Figure 2.6: Predicted longitudinal attenuation per meter for β=3; the parameter is γ_L.

2.3 Attenuation of Torsional Waves by a Layer of Dynamic absorbers

Finally we consider the same rod with a layer of dynamic absorbers to understand the effect of dynamic absorbers on torsional waves.

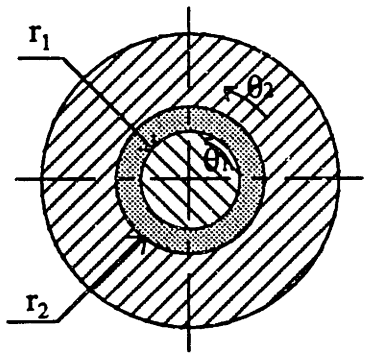

Figure 2.7: Side view of a semi-infinite circular rod with a dynamic absorber layer.

The coupled equations of motion are

$$-GI_1\frac{\partial^2\theta_1}{\partial x^2} + I_1\frac{\partial^2\theta_1}{\partial t^2} + R_T\frac{\partial}{\partial t}(r_1\theta_1 - r_2\theta_2) + k_T(r_1^2\theta_1 - r_2^2\theta_2) = 0 \tag{2.14}$$

$$I_2\frac{\partial^2\theta_2}{\partial t^2} + R_T\frac{\partial}{\partial t}(r_2\theta_2 - r_1\theta_1) + k_T(r_2^2\theta_2 - r_1^2\theta_1) = 0 \tag{2.15}$$

where I_1 and I_2 are the polar moments of inertia of the beam and the absorber; G the shear modulus of elasticity of the rod; R_T and k_T the per unit area resistance and stiffness respectively of the layer; θ_1 and θ_2 the angular displacement of the rod and attached mass respectively, as shown in Fig 2.7.

Consider $r = (r_1 + r_2)/2$. If the resilient layer is thin compared to the radius of the beam, then we have $r \approx r_1 \approx r_2$. Using this approximation, the equations of motion (2.14) and (2.15) become

$$-GI_1\frac{\partial^2\theta_1}{\partial x^2} + I_1\frac{\partial^2\theta_1}{\partial t^2} + R_T r\frac{\partial}{\partial t}(\theta_1 - \theta_2) + k_T r^2(\theta_1 - \theta_2) = 0 \tag{2.16}$$

$$I_2\frac{\partial^2\theta_2}{\partial t^2} + R_T r\frac{\partial}{\partial t}(\theta_2 - \theta_1) + k_T r^2(\theta_2 - \theta_1) = 0 \tag{2.17}$$

These equation of motion are seen to have the same form as the equations of motion previously obtained for the propagation of longitudinal waves.

We now seek solutions to Eq. (2.16) and (2.17) of the form

$$\theta_1 = \exp(iK_T x - i\omega t) \tag{2.18}$$

Similarly, we find that harmonic waves exist if

$$K_T^2 = \kappa_T^2\left[1+\beta\frac{\gamma_T + i\omega_{0T}^2/\omega^2}{\gamma_T + i(\omega_{0T}^2/\omega^2 - 1)}\right] \tag{2.19}$$

where $\beta = \frac{m}{M}$ the mass ratio

$\gamma_T = \frac{R_T}{\omega m}$ the loss factor of the dynamic absorber

$\omega_{0T}^2 = \frac{k_T r_2^2}{I_2}$ the square of the dynamic absorber's torsional resonance frequency

$\kappa_T = \frac{\omega}{c_T}$ the rod torsional wavenumber in the absence of the layer

and c_T is the torsional speed defined by

$$c_T = \sqrt{\frac{GS}{M}} \tag{2.20}$$

Similarly, the resulting attenuation per unit distance is

$$A_T = 20\log(e)K_T i = 8.686K_T i \quad \text{dB/unit of distance} \tag{2.21}$$

So using the assumption that the resilient layer is thin compared to the radius of the beam allows one to obtain similar equations as the in the longitudinal case. The curves representing the attenuation versus frequency are similar to the longitudinal ones, the only changing parameter being the speed of the wave which affects the amplitude of the attenuation.

3 Design of the Dynamic Absorbers

3.1 Preliminary Considerations

To apply the analytical models described in chapter 2, dynamic absorbers need to be defined by their mass, stiffness and loss factor. The mass is easy to predict, knowing the density and the geometry of the piece of material. The stiffness and the loss factor are much more difficult to predict although some studies have been made on the subject [6]. As a consequence an experiment has been designed to measure these characteristics. The procedure followed is inspired by Richard Sapienza [7].

The objective is to build dynamic absorbers which will have an effect on the truss. The resonance frequency, influenced by the mass and the stiffness, has to be high enough so that strong motion exits on the rods. Some practical considerations, developed in chapter 4, limit the use the foregoing models at high frequencies. Basically, if the resonance frequency is high, more dynamic absorbers are required to obtain a continuous distribution necessary to apply the analytical model.

3.2 Mechanical Design

Each dynamic absorber mass is built in two semi circular pieces so that it is easily put on and removed from the structure. Aluminium is chosen for the material to facilitate the manufacturing process. The symmetry is respected to prevent side effect resonances. A base wide enough compared to the outer diameter is necessary to provide a decreased likehood of rocking motion and misalignment.

A mechanical drawing of the dynamic absorber mass is presented in Fig 3.1. The inner radius is larger than the radius of a typical rod used to build the truss so that the resilient material can be added between the rod and the circular mass. The outer radius and the base of the circular mass define the geometry (i.e. the mass) of the dynamic absorber.

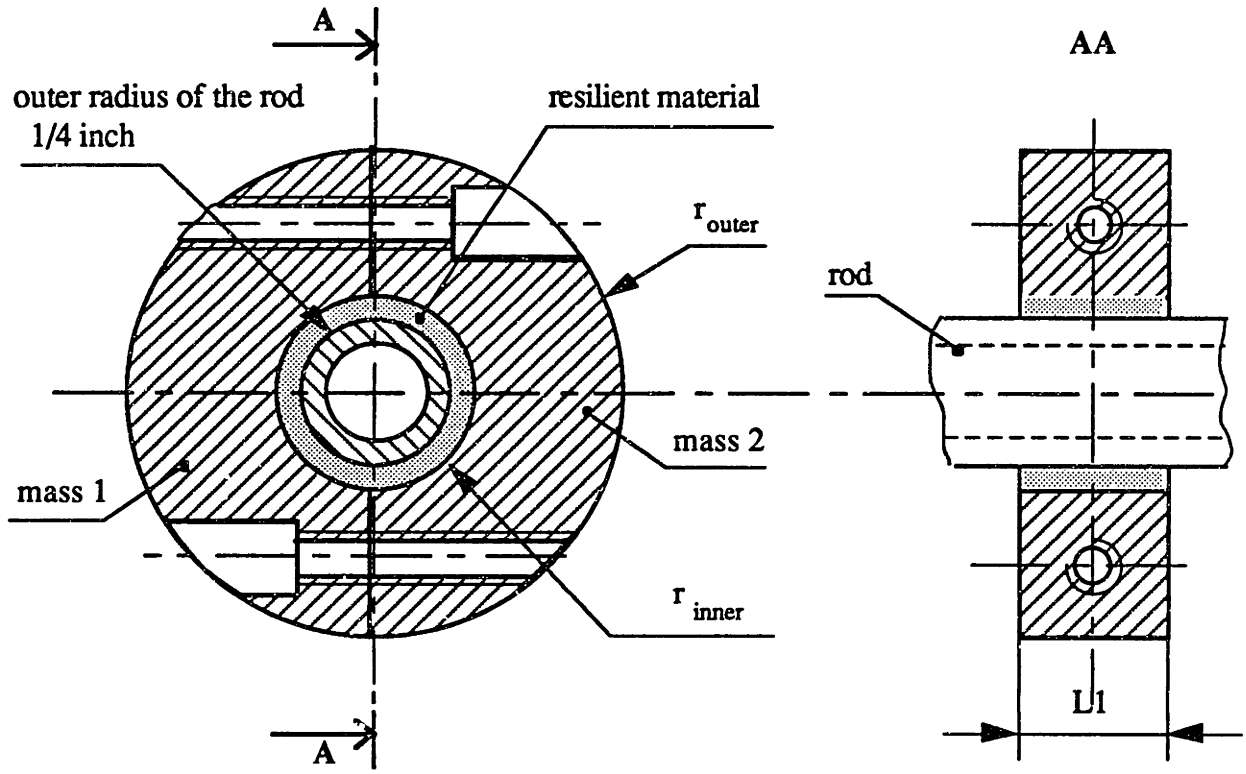

Figure 3.1: Mechanical drawing of a dynamic absorber.

3.2 Measurement of the Resonance Frequencies

Longitudinal Resonance

The layer's longitudinal resonance is determined by using a single dynamic absorber resiliently mounted on a rod similar to the ones used for the full truss. The setup is shown on Fig 3.2. A control accelerometer is mounted as close to the mass as possible and a response accelerometer is mounted to the outer diameter of the mass. The PCB model 309A accelerometers are oriented in the direction defined by the main axis of the rod and attached to the components with bees wax. A PCB 483B07 ICP signal conditioner provides the voltage supply and amplification for the two sensors. The rod is hung horizontally by means of monofilament lines with the input excitation supplied by means of a Wilcoxon Research vibration generator (model F3/F9). Mounting of the shaker to the rod is accomplished by adding a small aluminium plate, center drilled, tapped and fitted with a mounting stud at the end of the rod. By tightening the shaker down on the mounting stud, axial alignment is ensured, reducing possible coupling to flexural motion. The shaker is

driven by a signal from a HP 3562A two channel dynamic signal analyzer with the source option active. The input is band limited white noise. The analyzer is used to power the accelerometers, as well as for signal analysis. The transfer function between the input and response acceleration in the longitudinal direction is used to determine the longitudinal resonance frequency and loss factor at resonance.

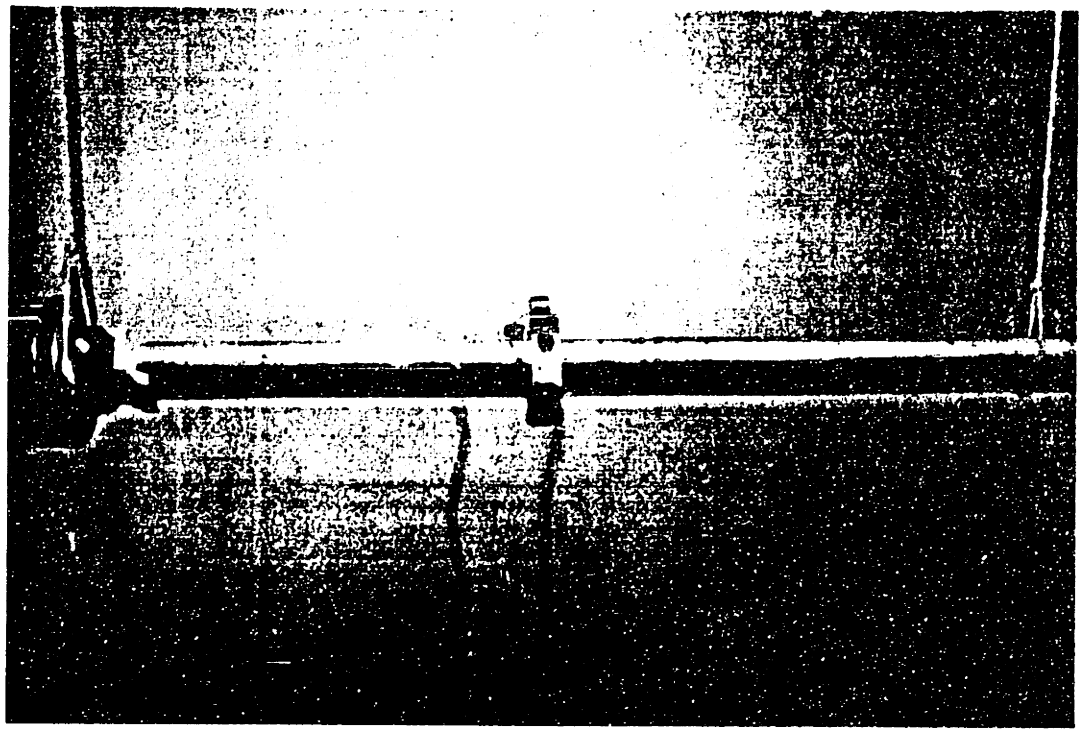

Figure 3.2: Photograph of longitudinal mass resonance apparatus.

Flexural Resonance

The layer's flexural resonance is also determined by using a single dynamic absorber resiliently mounted on a rod similar to the ones used for the full truss. The accelerometers, amplifiers and analyzers remain the same but the setup is different and shown in figure 3.3. A fixed shaker is attached to a special piece of aluminium designed for the experiment. The excitation, perpendicular to the tube axis, is transmitted at each end of the small rod. This creates a symmetric excitation and insures that the dynamic absorber only moves in the direction perpendicular to the tube axis. The input is also band limited white noise. The transfer function between the input and response acceleration in the normal direction is used to determine the flexural resonance frequency and loss factor at resonance.

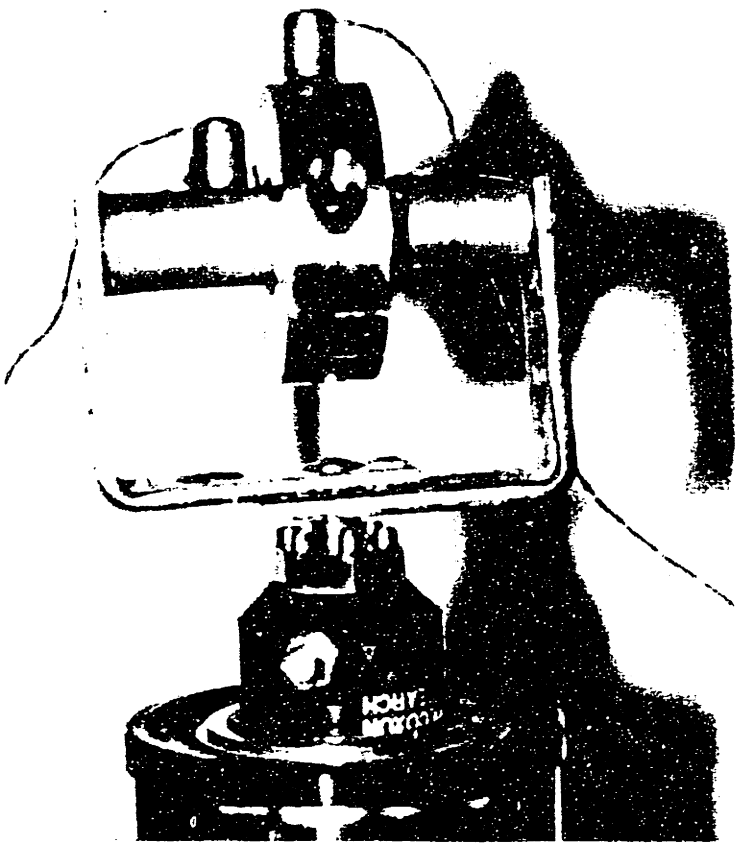

Figure 3.3: Photograph of flexural mass resonance apparatus.

3.4 Results

Different materials such as weatherstriping and neoprene of different durometers have been tested to attach the masses on the tubes. Different sizes for the masses have also been tested.

Measurements of the resonance frequencies and loss factors were performed as described in section 3.3. The resonance frequency f_0 is defined as the frequency at the transfer function peak. The loss factor is determined by the 3dB bandwidth of the transfer function and is given by the equation

$$\gamma = \frac{\Delta f_{3dB}}{f_0} \tag{3.1}$$

A dynamic absorber made of weatherstriping and a mass of 38g was selected as satisfactory. The inner radius is 0.25 inch + 1mm, the outer radius is 0.75 inch and the base is 0.5 inch. The weatherstriping is squeezed between the two masses and the rod. The

flexural and longitudinal resonances of this dynamic absorber are approximatly the same (437 Hz and 447 Hz) and fill the conditions defined at the beginning of this chapter. The mass of this dynamic absorber allows one to create a mass ratio of approximatly three on the different kinds of finite rods used on the full truss (see next chapter for more details).

As the resonance frequency and the loss factor depend on parameters such as temperature, time relaxation of the resilient material and operator manipulations such as the way the resilient material is squeezed, many tests were completed to obtain averaged values. The results are shown in Tables 3.1 and 3.2. The transfer functions corresponding to Test #1 and Test #6 are shown on Fig 3.4 and Fig 3.5 .

	Test #1	Test #2	Test #3	Test #4	Test #5	Mean
f_{0f} (Hz)	417	416	477	452	422	437
γ_F	0.18	0.20	0.19	0.18	0.19	0.19

Table 3.1: Flexural characteristics

	Test #6	Test #7	Test #8	Test #9	Test #10	Mean
f_{0L} (Hz)	448	481	415	430	461	447
γ_L	0.34	0.36	0.37	0.33	0.34	0.35

Table 3.2: Longitudinal characteristics

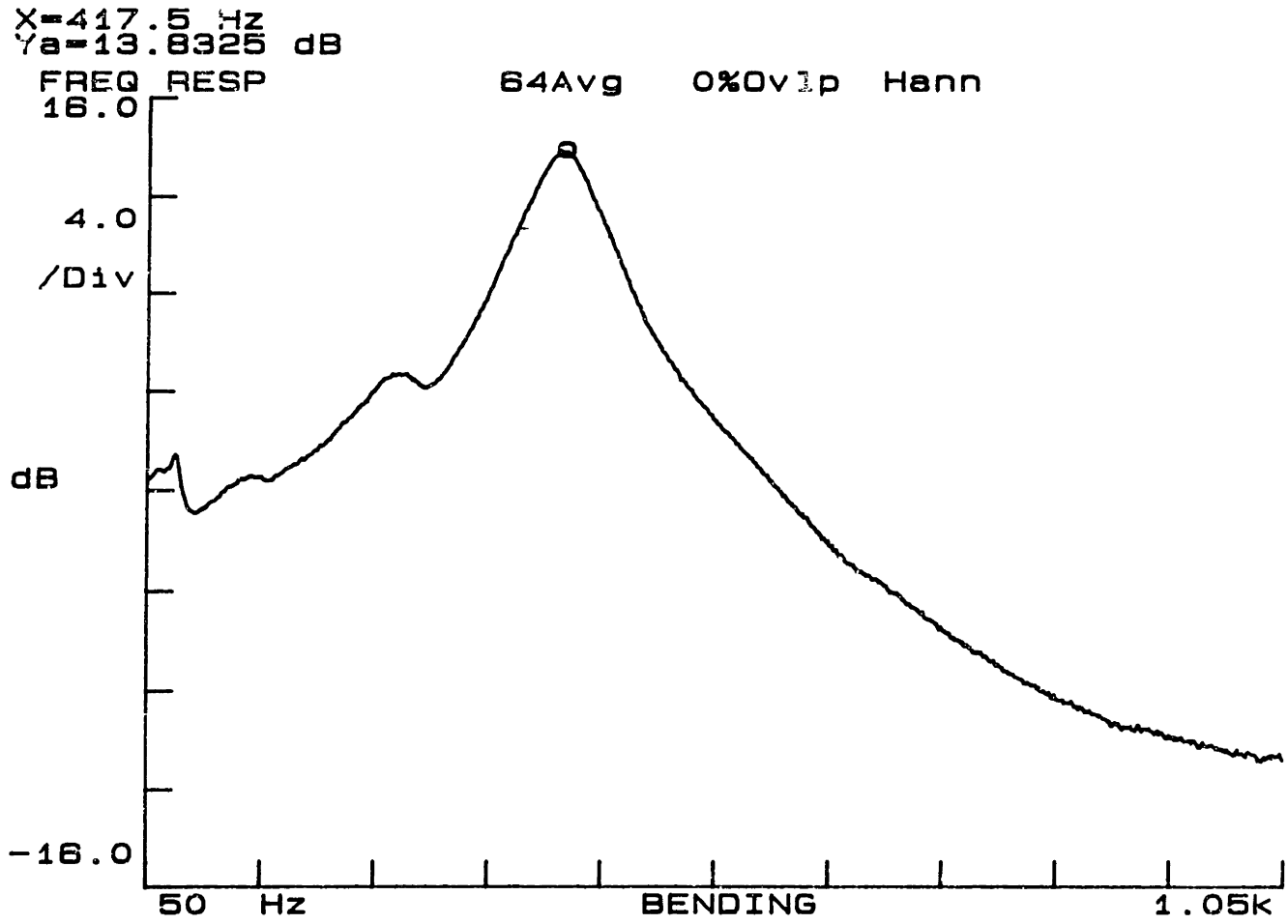

Figure 3.4: Transfer function of Test #1.

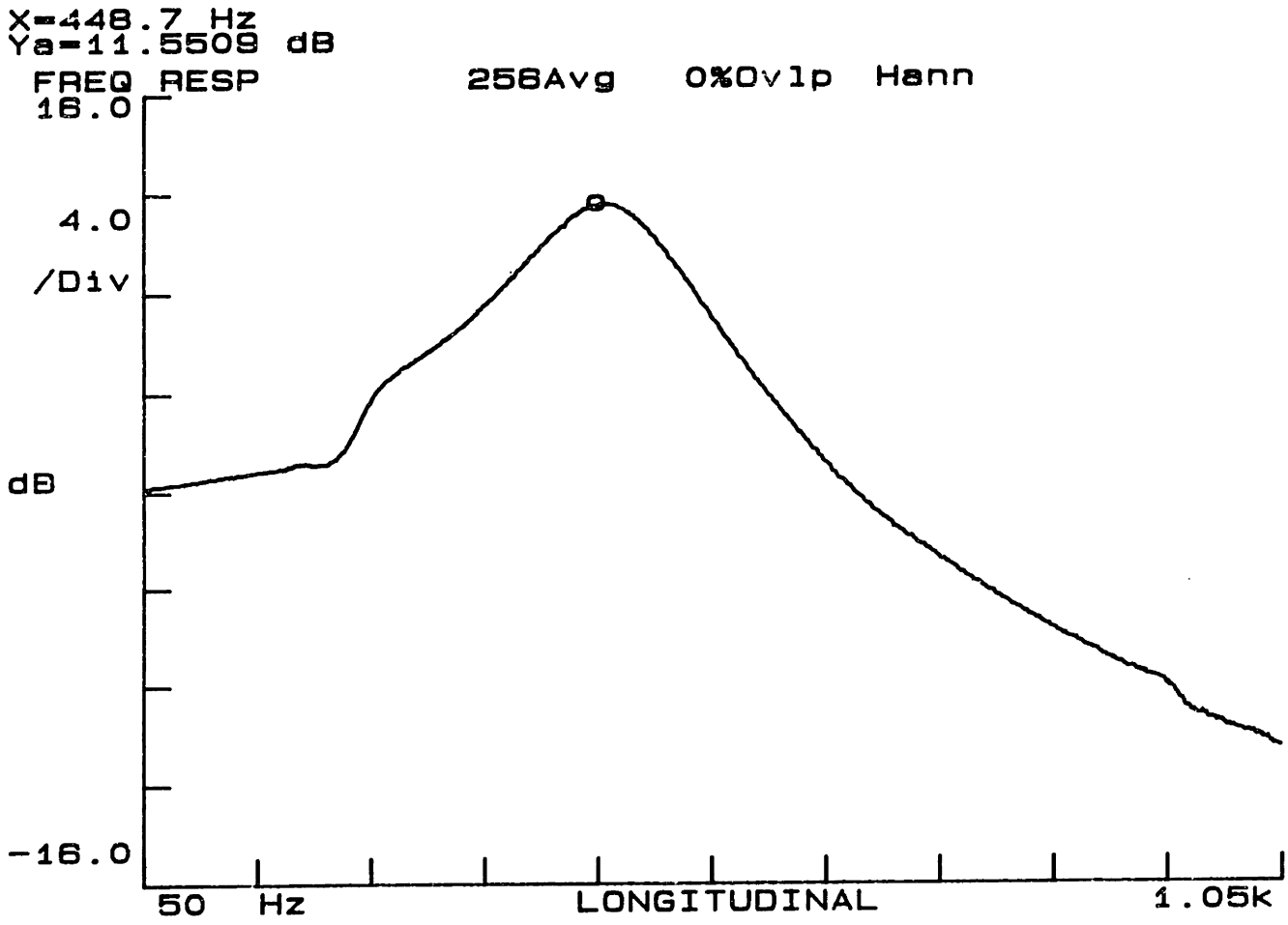

Figure 3.5: Transfer function of Test #6.

3.5 Torsional Resonance Frequency

The rods used for the truss are 1/2 inch diameter. The equipment necessary to measure the angular displacement is not available at MIT. So for practical reasons, the torsional resonance could not be measured. However, a simple model is shown here to estimate the torsional resonance frequency.

For flexural resonance, the strain of the resilient material is a complicated combination of compression and shear which is not well adapted to analysis. But for longitudinal and torsional movement, the physical process of deformation of the resilient material is of the same nature [6]. As a consequence, the stiffness can be considered as equivalent in both cases.

The longitudinal resonance is given by

$$\omega_{0L} = \sqrt{\frac{k_L}{m}} \tag{3.2}$$

and the torsional resonance is given by

$$\omega_{0T} = \sqrt{\frac{k_T r_{inner}^2}{m\chi_{abs}^2}} \tag{3.3}$$

where χ_{abs} is the radius of giration of the mass, defined by $\chi_{abs} = \frac{1}{2}\sqrt{r_{inner}^2 + r_{outer}^2}$

Making the assumption that the stiffness is the same in (3.2) and (3.3) and combining the two equations, we find

$$\omega_{0T} = \omega_{0L}\sqrt{\frac{r_{inner}^2}{\chi_{abs}^2}} \tag{3.4}$$

or

$$f_{0T} = f_{0L}\frac{r_{inner}}{\chi_{abs}} \tag{3.5}$$

For the design shown in Fig 3.1, we have $r_{inner} = 0.735$ cm and $\chi_{abs} = 1.02$ cm, so $f_{0T} = 330$ Hz.

4 Experiment

4.1 Preparation and Preliminary Considerations

The experimental model was designed, built and used by Marcus Heath. It is a truss consisting of eleven square-based pyramids joined in series. It is fabricated from 6061 T6 aluminium joints and rods, and has a mass of 16 kg. The architecture of the truss is represented in Fig 4.1. Details of truss design, construction and material properties are to be found in [1]. Although scaling provides some degree of applicability to the model, the truss is not architectured as a feasible internal structure, but as a model allowing to understand the dynamics of a three dimensional truss. The length of the truss has been selected to maximize the axial dimension so that attenuation is readily measurable.

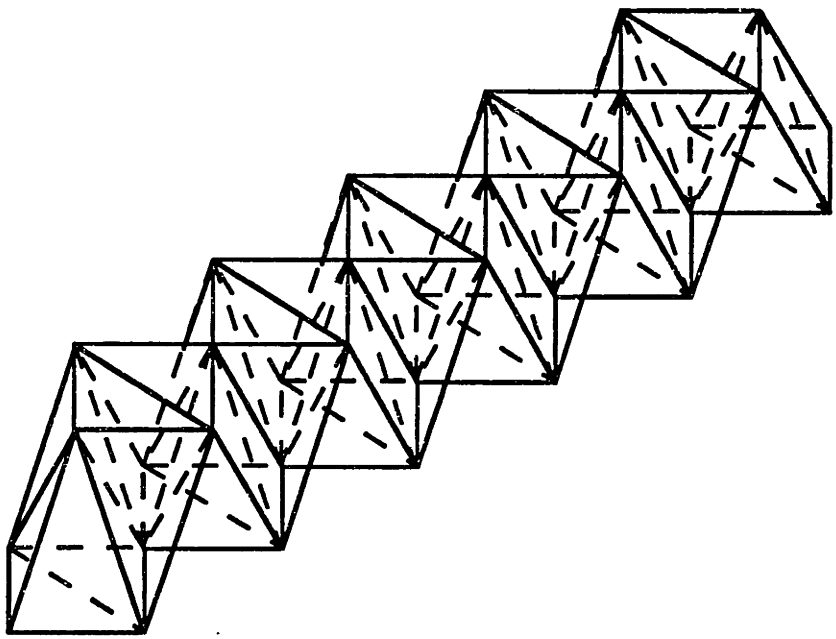

Figure 4.1: Architecture of the truss.

The truss is suspended from the laboratory ceiling using two bungee chords. The natural frequency of rigid body oscillation is of the order of 10 Hz so that the truss is considered to be suspended in free space for frequencies above 100 Hz, i.e. for the frequency range of this experiment. The two supports are attached at intermediate positions

along the truss in order to minimize hogging or sagging effects. The axial direction of the truss is considered the X direction, Y extends in the horizontal transverse direction and Z represents the vertical transverse direction.

The dynamic absorbers are added on the truss as shown on Fig 4.2 .

Figure 4.2: Attachment of dynamic absorbers on the structure.

The first parameter which affects the spacing of the absorbers is the mass ratio β. We recall in Chapter 2 that the dynamic absorbers create an attenuation band approximately defined by

$$1 < \omega/\omega_0 < \sqrt{1+\beta} \tag{2.6}$$

For $\beta = 3$, the attenuation band is limited by f_0 and $2f_0$. In our case, the resonance frequency is 450 Hz for longitudinal and flexural waves; a mass ratio of 3 creates an attenuation band between 450 and 900 Hz. $\beta = 3$ is arbitrarily selected as satisfactory. A dynamic absorber has a mass of 38 g and the mass per length of the tubes is 0.154 g/m so the spacing d is defined by

$$d = \frac{0.038}{3 \times 0.154} = 0.082 \text{ m} \tag{4.1}$$

The attachment spacing of the absorbers also has to be such that the continuous distribution required to apply the analytical model is satisfied. As a rule of thumb [7], a minimum of four masses per wavelength satisfies the continuity criteria. Consider the flexural waves which have the smallest wavelengths in the frequency range considered. λ_f is given by

$$\lambda_f = \sqrt{2\pi\chi c_L}\,\frac{1}{\sqrt{f}} \tag{4.2}$$

where χ is the radius of giration, c_L the longitudinal wave speed and f the frequency.

For a spacing of d = 0.082 m, the continuity criteria is valid up to $\lambda_f = 4d = 0.33$ m. This critical wavelength corresponds to a critical frequency f_{cr} defined by

$$f_{cr} = \frac{2\pi \times 0.004 \times 5091}{0.33^2} = 1180 \text{ Hz} \tag{4.3}$$

In conclusion, if the dynamic absorbers are added on the tubes every 8.2 cm, the mass ratio is three, then the continuity criteria for flexural waves is valid up to approximately 1200 Hz. The exact spacing used in the experiment is discussed in 4.3.

4.2 Equipment

To simulate the vibration caused by rotating machinery, a vibration generator is fixed to an end joint (joint b1) by means of a mounting stud. Located at one extreme end, the shaker maximizes the available length of measurement. A Bruel and Kjaer type 4810 vibration generator is used to excite the truss in frequency bands over the desired frequency range of 80 Hz to 12 kHz. This shaker applies sufficient force to maintain a signal to noise ratio of at least 25 dB throughout the truss. This shaker incorporates an external force transducer for transfer function measurements.

Twelve PCB model 309A internally amplified accelerometers are attached to the truss components with bees wax. The PCB sensors weighing 1 gram have a negligible effect on the level of vibration of the joints (a joint has a mass of 120 grams [1]). A twelve channel PCB 483B07 ICP signal conditioner provides the voltage supply and amplification for the twelve sensors. The twelve amplified channels become input to a HP 3562A two channel dynamic signal analyzer. Each measurement requires to switch from one amplified channel to the next one.

4.3 Procedure

Dynamic absorbers are added on a section in the middle of the truss so that no wave can propagate from one part to the other without going through a treated rod. In this first configuration called 'half damped', seven tubes are treated. This configuration is represented in Fig 4.3. Four 20 inch long tubes receive 6 equally spaced dynamic absorbers. On these tubes $\beta = 2.91$, $d = 7.3$ cm and $f_{cr} \approx 1500$ Hz. Three 33 inch long tubes receive 10 equally spaced dynamic absorbers. On these tubes $\beta = 2.94$, $d = 7.6$ cm and $f_{cr} \approx 1400$ Hz. A total of 54 dynamic absorbers are added to the truss.

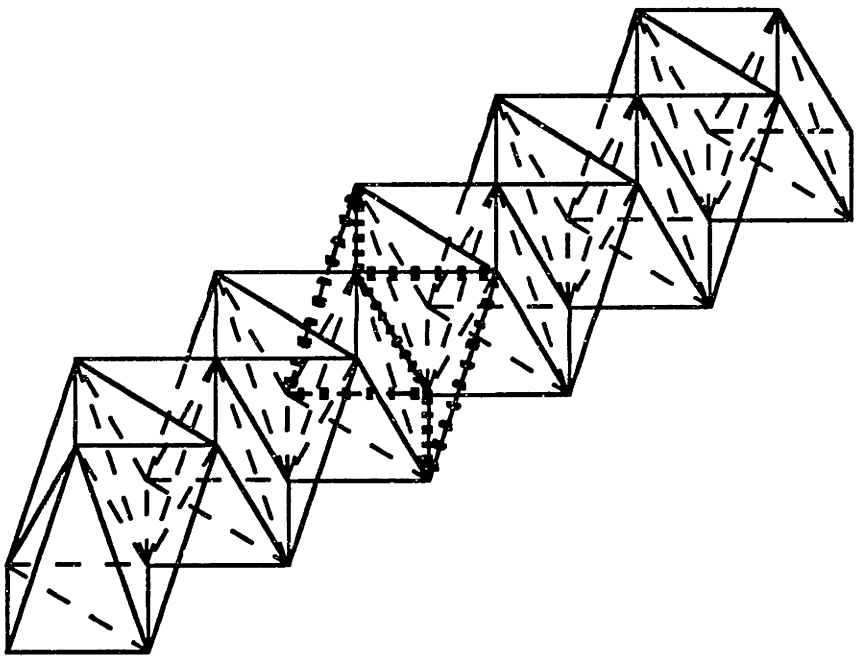

Figure 4.3: Half damped configuration.

In a second configuration called 'fully damped', six additional tubes are treated. This configuration is represented in Fig 4.4. Four 33 inch long tubes receive 10 equally spaced dynamic absorbers (same characteristics as in the first configuration). Two opposite 29 inch long tubes receive 8 dynamic absorbers. On these tubes $\beta = 2.68$, $d = 8.2$ cm and $f_{cr} \approx 1200$ Hz. 110 dynamic absorbers are required for this second configuration.

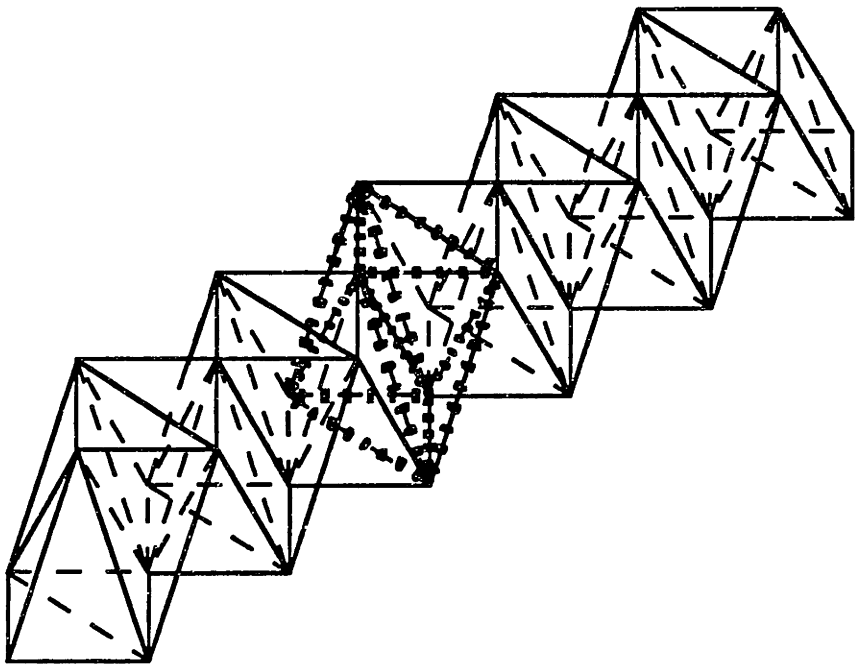

Figure 4.4: Fully damped configuration

The procedure for the measurements is the same than the one followed by Marcus Heath for the measurement of the steady state attenuation of acceleration as a function of axial distance [1]. As a consequence, data from the undamped structure can be compared to data acquired from the treated structure.

In a first experiment, a random force signal in proportional frequency bands, ranging from the 125 Hz to the 8 kHz octave, excites the truss. The excitation of only one band at a time permits data acquisition within the band while maximizing the power available to the vibration generator. The HP 3562 dynamic signal analyzer generates the band passed signals and acquires and processes data.

In a second procedure, attention is focused on narrow frequency bands from 350 Hz to 750 Hz.

In each case and for each band, the steady state accelerance of every joint is measured and recorded in dB re 1g/N. The data are presented in the frequency domain and many sets of data are averaged to reduce response fluctuations. At high frequencies 32 averages are conducted; at low frequencies 3 averages are conducted. Although this is a small number of averages, at low frequencies additional averages do not really improve the quality of the signal. A linear average of all processed accelerance data within each band (expressed in dB) is executed to obtain a single averaged value. To obtain the overall effect of axial attenuation, the response in dB of each three joint grouping per section is linearly averaged.

This effectively smooths variations over one section. Finally, the accelerance data are normalized by the the response measured at the first joint near the shaker.

To summarize, the attenuation in acceleration with reference to the first section is measured for each section and is given in dB.

4.4 Results

The attenuation is measured for the half damped and the fully damped configuration. This attenuation is compared with data obtained by Marcus Heath for the undamped truss in similar conditions. The difference between the curves show the effect of the dynamic absorbers. The difference between the half damped and undamped truss is plotted on Figs 4.5 and 4.6. The difference between the fully damped and undamped truss is plotted on Figs 4.7, 4.8 and 4.9.

The analysis of these curves is done in Chapter 5.

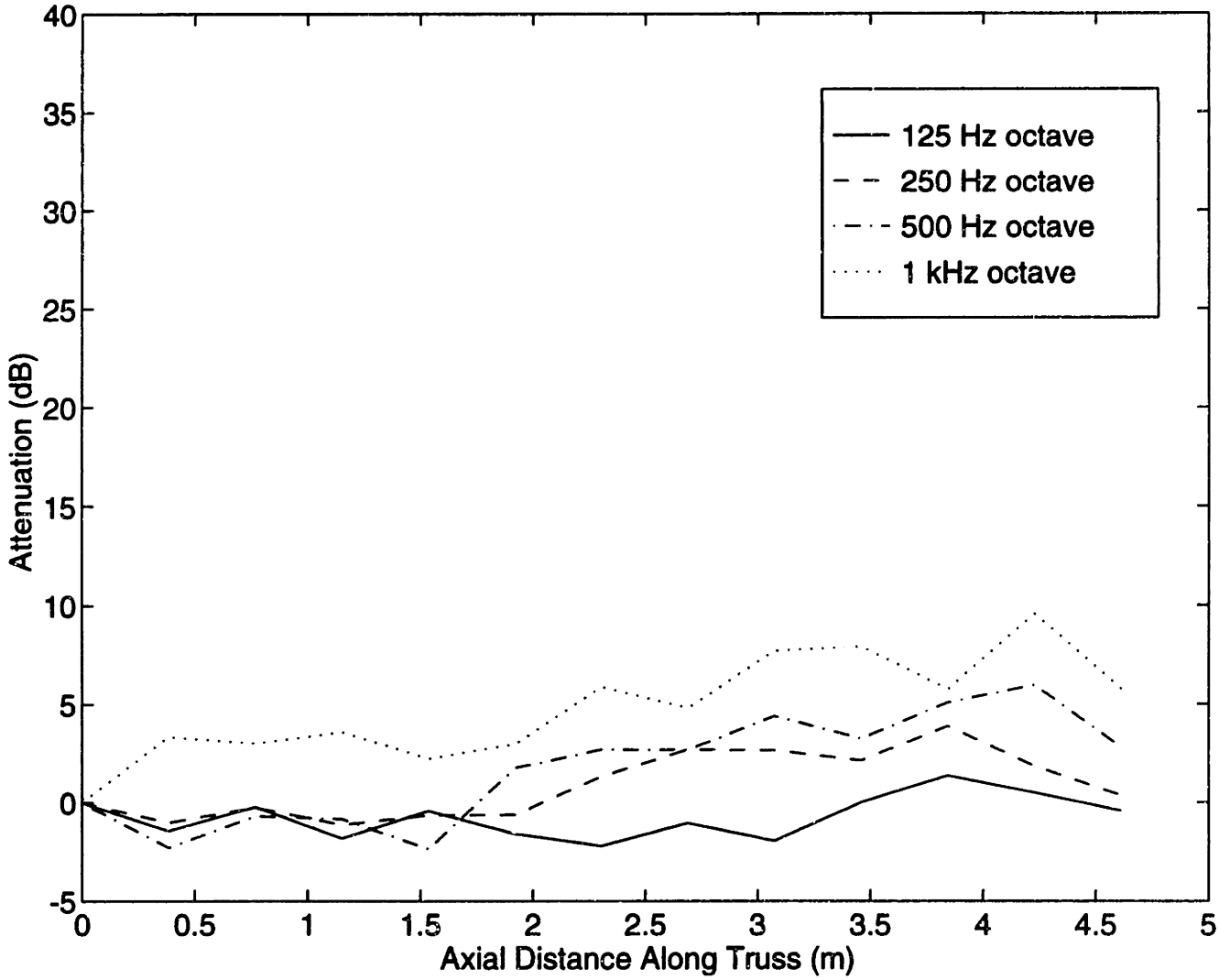

Figure 4.5: Difference of attenuation versus axial distance at low frequencies between the half damped and the undamped configuration.

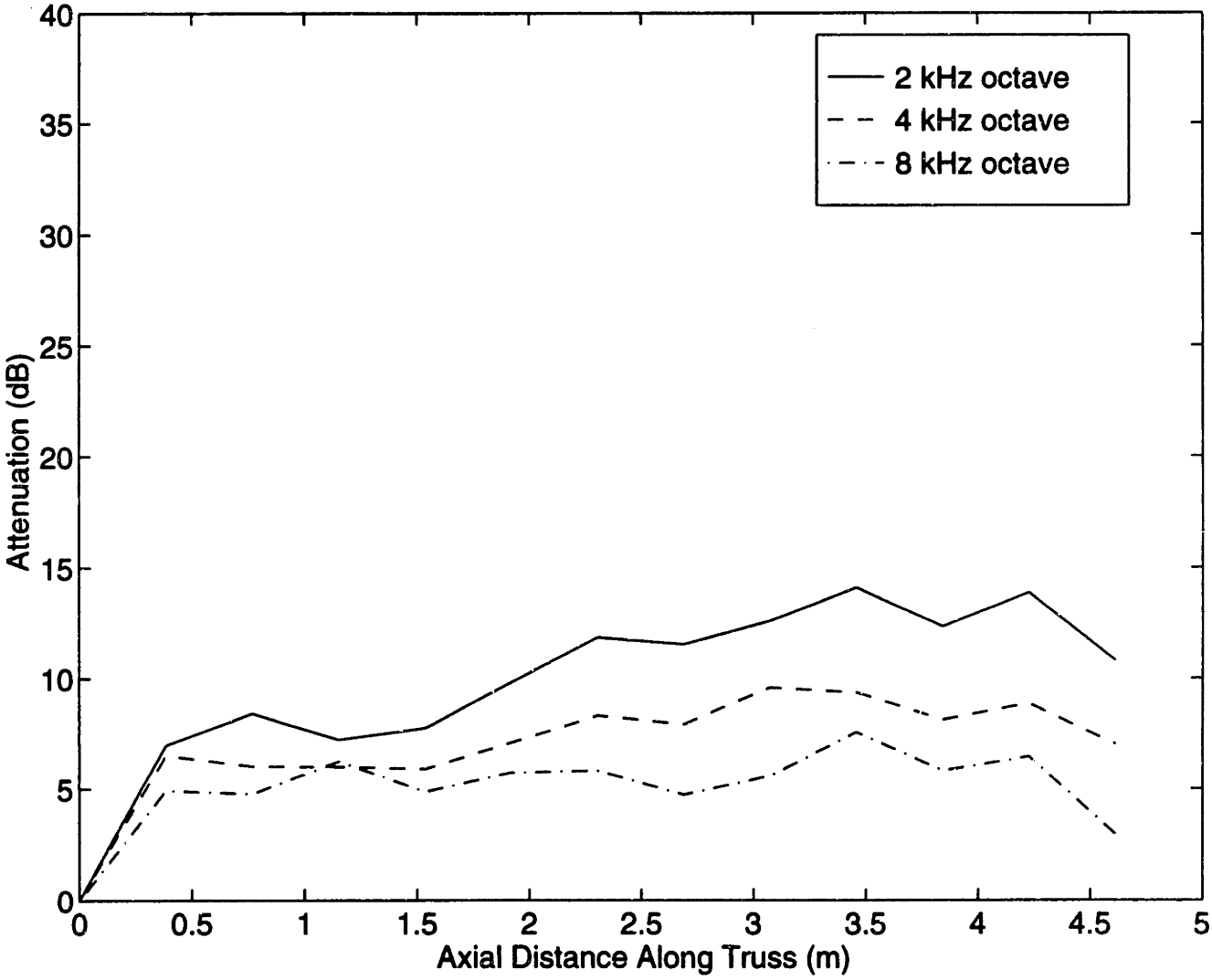

Figure 4.6: Difference of attenuation versus axial distance at high frequencies between the half damped and the undamped configuration.

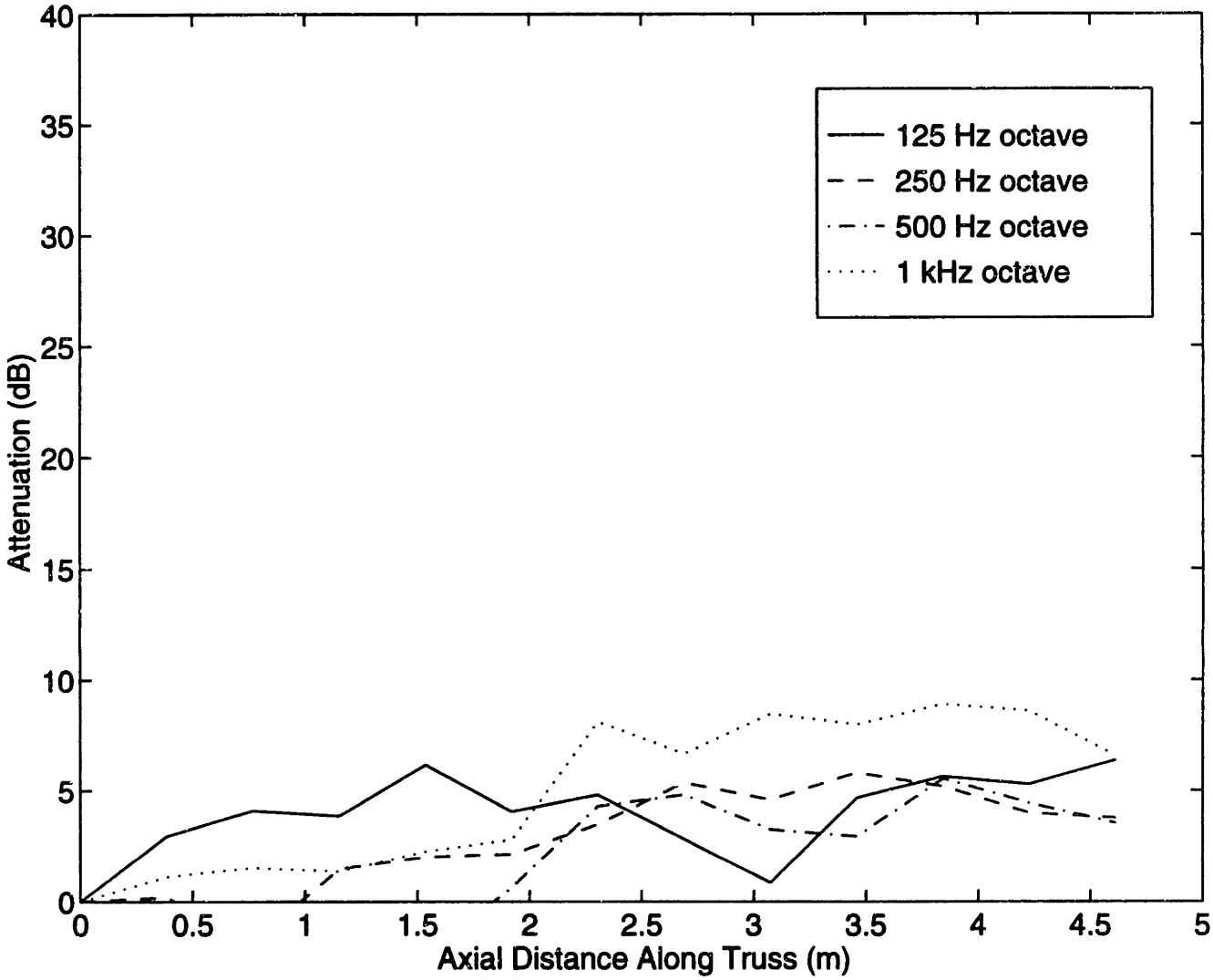

Figure 4.7: Difference of attenuation versus axial distance at low frequencies between the fully damped and the undamped configuration.

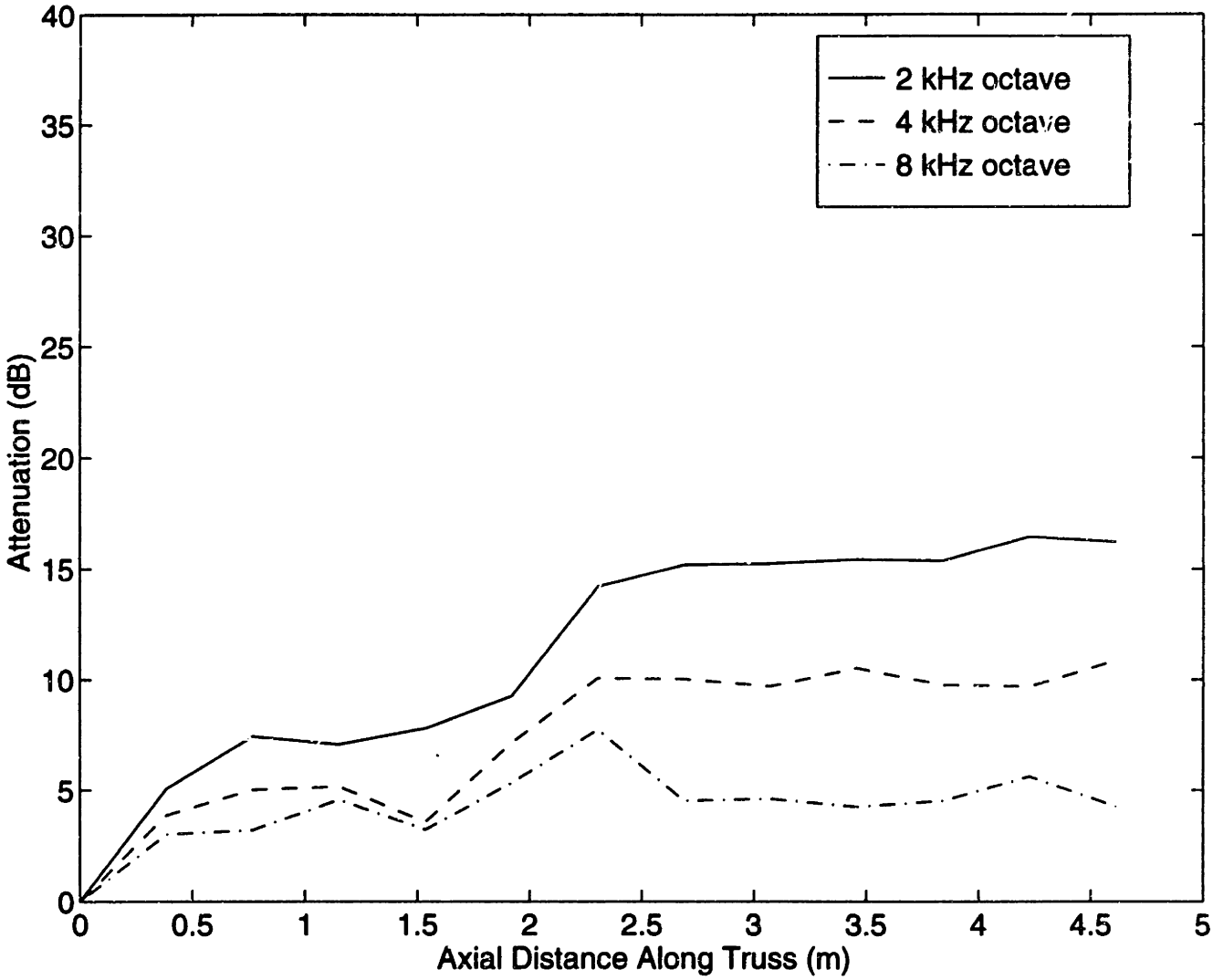

Figure 4.8: Difference of attenuation versus axial distance at high frequencies between the fully damped and the undamped configuration.

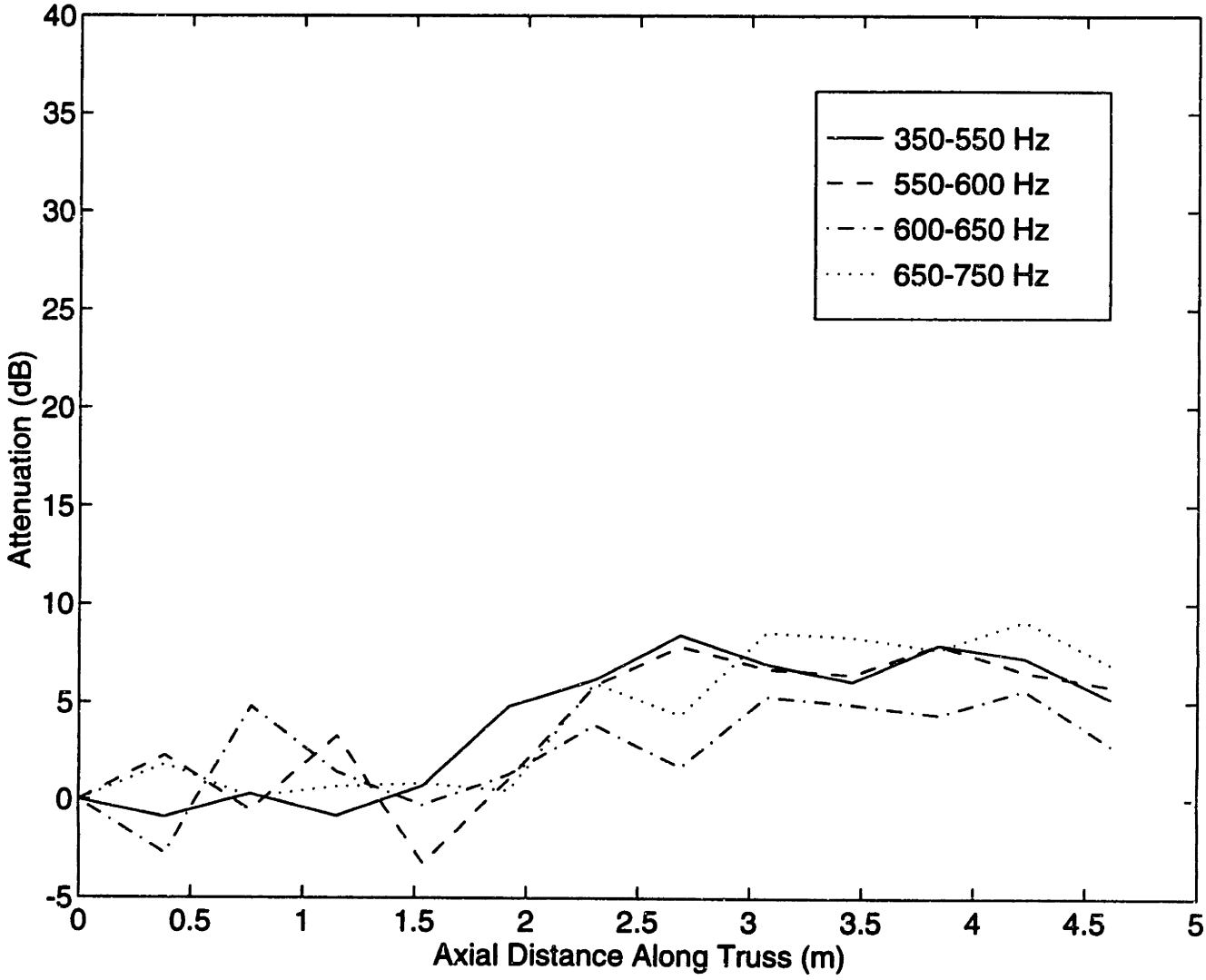

Figure 4.9: Difference of attenuation versus axial distance at middle frequencies between the fully damped and the undamped configuration.

5 Analysis

In this chapter, the measured axial attenuation along the truss is compared to analytical predictions. Differences in the shape of the curves question the assumptions made for the prediction of axial attenuation and the validity of the analytical models of Chapter 2. Section 5.3 is introduces a new model which takes into account finite boundary conditions. In Section 5.4, the solution obtained with this new model is compared to an experiment to prove its validity. Section 5.5 deals with the behavior of dynamic absorbers at high frequencies. As experimental data show a higher level of attenuation than expected at high frequencies, mechanisms of attenuation and of reflection are proposed when the continuity criteria of the layer is no longer valid, which is the case above 1200 Hz for flexural waves.

5.1 Analysis of the Experimental Curves

For all configurations, the dynamic absorbers are located at a distance of 1.9 to 2.4 meters from the vibration source. The overall shape of the experimental curves of attenuation versus distance is a step function, with the step located in the dynamic absorbers attachment area. The step is dramatic for frequency bands ranging from the 250 Hz octave band to the 4 kHz octave band. For low frequencies, the attenuation due to dynamic absorbers is no significant.

The difference between the half damped configuration and the fully damped configuration is not significant. This means that the main effect of the dynamic absorbers is to separate the truss in two parts with two different levels of vibrations. To simplify the representation, the experimental curves corresponding to the half damped configurations are averaged over each section separated by the dynamic absorber "filter". These curves are presented in Figs 5.1 and 5.2.

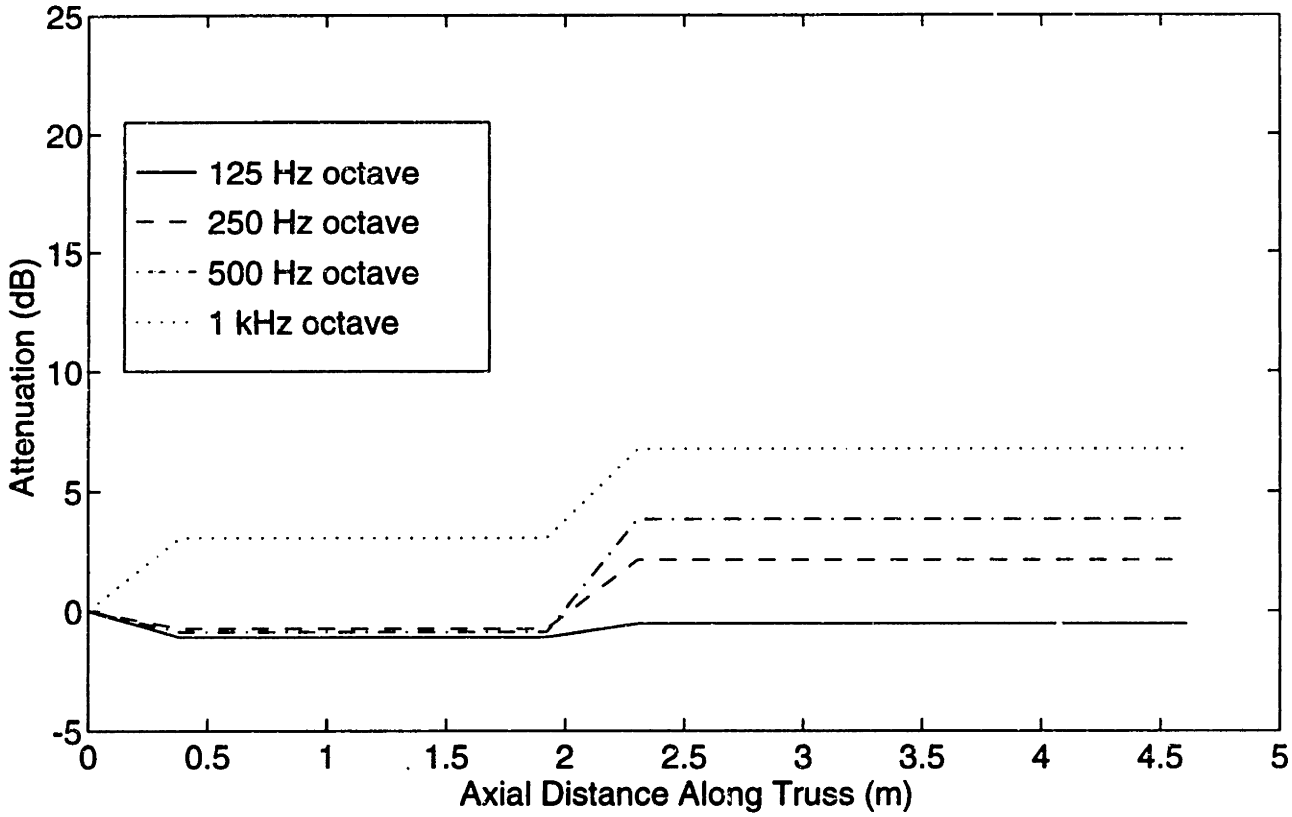

Figure 5.1: Averaged attenuation versus axial distance at low frequencies for the half damped case.

The 125 Hz octave band curve is flat and remains equal to zero along the truss; the dynamic absorbers do not attenuate waves at low frequencies. However, the attached masses probably have an effect on the global motion of the truss as shown on Fig 4.7. The configuration can be depicted as a beam with an added mass at the center. This added mass increases the level of attenuation at the center of the beam.

The 250 Hz and 500 Hz octave band curves show clearly a step function. In the 250 Hz octave band, mostly torsional waves are expected to be absorbed. In the 500 Hz octave band, the three types of waves are absorbed, resulting in a bigger step of 5 dB.

The 1000 Hz octave band is a double step function. The first step of 3 dB occurs near the source. The second step of 3 dB occurs in the dynamic absorbers area. This same trend exists for the 2 kHz and 4 kHz octave bands.

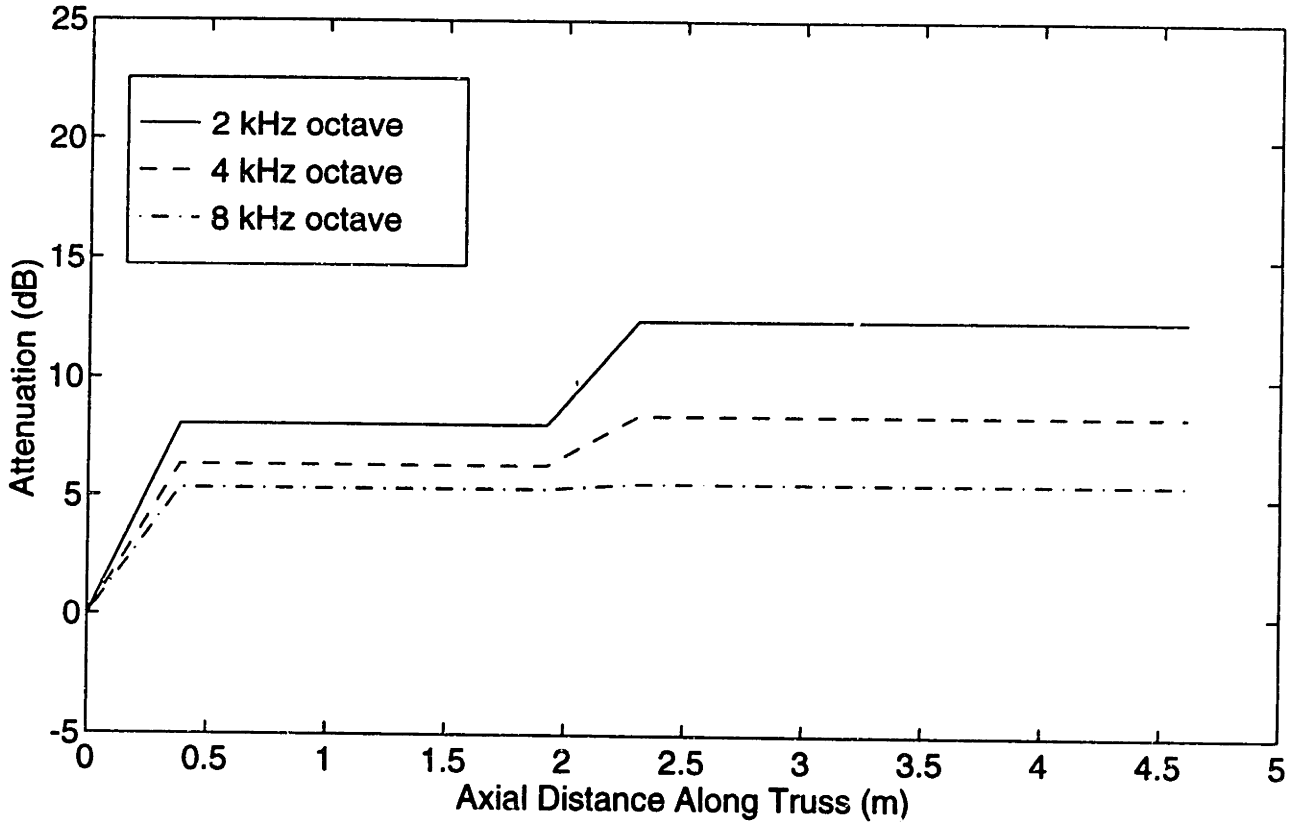

Figure 5.2: Averaged attenuation versus axial distance at high frequencies for the half damped case.

For the 8 kHz octave band, the second step disappears. The level of attenuation is 5 dB all along the truss, except near the source. The dynamic absorbers no longer separate the truss in two parts with two different levels of vibration.

5.2 Analytical Predictions

The dynamic absorbers added to the structure have a flexural and longitudinal resonance frequency of 450 Hz, and a torsional resonance frequency of 330 Hz. The attenuation per meter of a semi-infinite rod for the different types wave types is plotted in Fig 5.3. These analytical curves, based on the models discussed in Chapter 2, predict a strong attenuation between 300 Hz and 1 kHz. These curves can be used to predict the axial attenuation along the truss given assumptions described in the following section.

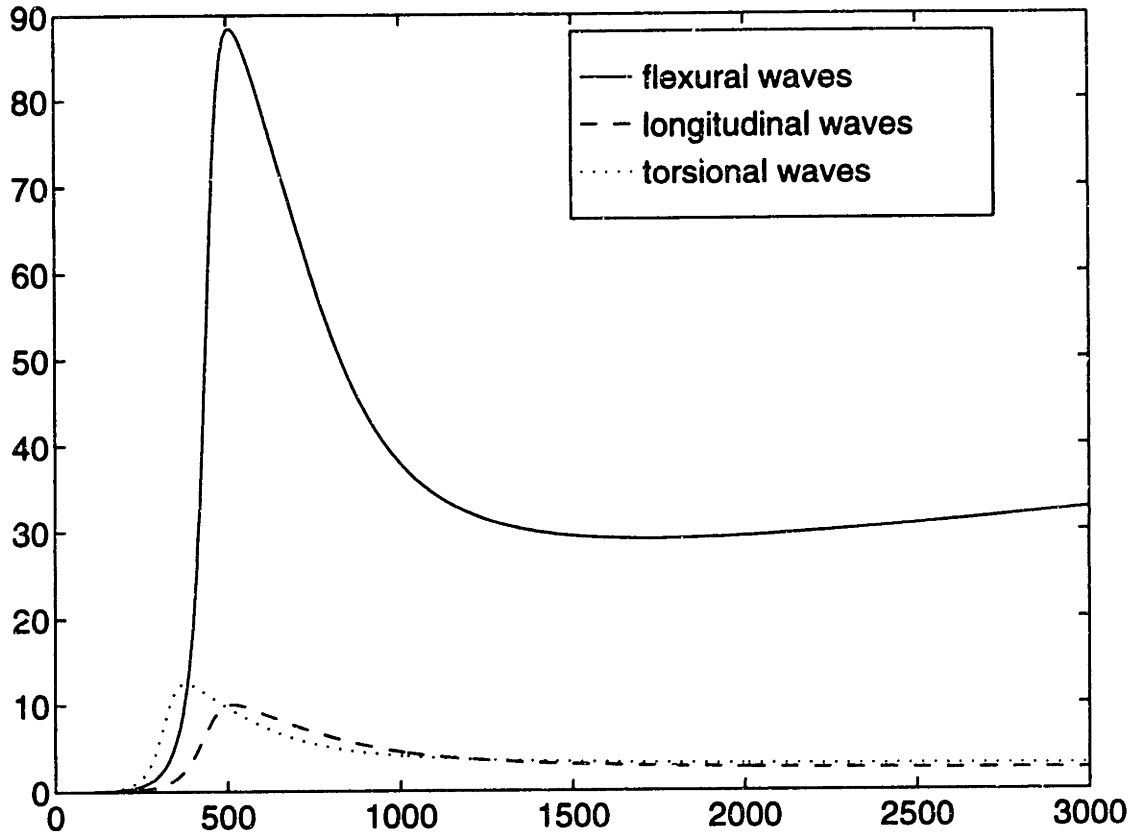

Figure 5.3: Attenuation per meter versus frequency of flexural, longitudinal and torsional waves for a semi-infinite rod.

A wave travelling across the treated section of the half damped truss has 7 path options: either one of the four 50 cm long rods or one of the three 84 cm long rods. An equivalent treated distance can be defined as the mean distance a wave is expected to cover on treated rods. For this configuration the equivalent distance can be defined as

$$\text{equivalent distance} = \frac{50\times4 + 83\times3}{3+4} \approx 65 \text{ cm} \tag{5.1}$$

For each wave, the accelerance corresponding to the attenuation suffered on a 65 cm long rod can be evaluated versus frequency and averaged on octave bands. The averaged values are plotted on Fig 5.4.

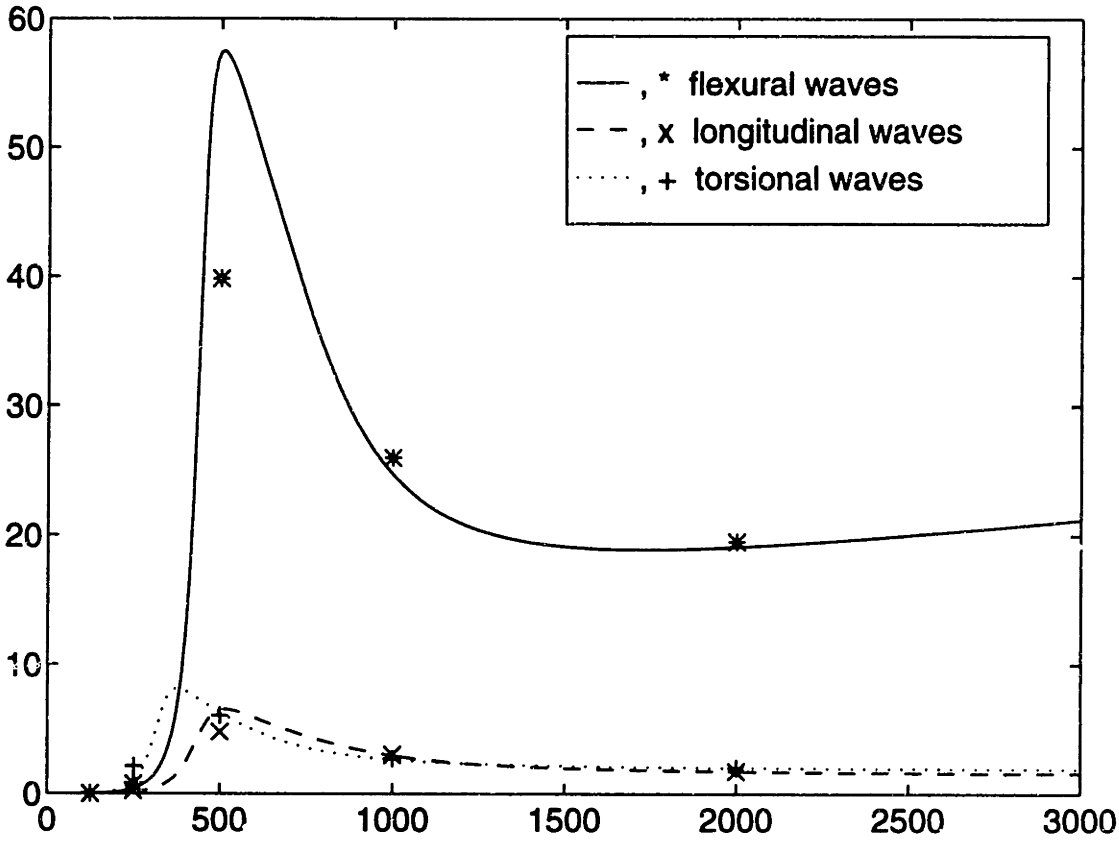

Figure 5.4: Attenuation versus frequency of flexural, longitudinal and torsional waves after 65 cm of treated rod and corresponding averaged values on octave band.

To predict the total axial attenuation along the truss, two assumptions are required. First, I assume that the transfer functions of the different accelerances from the rods to the joints are independent of wave type and frequency. This means that attenuation suffered on the rod results in the same attenuation measured at the joints. Second, knowledge about the partition of mean square acceleration between the different kinds of waves is necessary. As this information is not available, I make the assumption of equi-partition of energy among all wave types. With some calculation, the partitioning of acceleration can be derived from this hypothesis.

Using these two assumptions, the axial attenuation along the truss can be evaluated for a right-travelling wave. I assume that the attenuation only takes place in the treated area and that the added dynamic absorbers do not influence the level of vibration before and after the

treated area. Therefore, the band-averaged attenuation for each wave type is multiplied by its partition coefficient and the antilog values are added to give the global attenuation along the truss, resulting in a step function. The curves obtained are shown on Fig 5.5.

First, I calculate the partitioning of acceleration assuming equi-partition of energy.

The total mean square acceleration in a given frequency band is

$$a^2 = a_f^2 + a_L^2 + a_T^2 \tag{5.2}$$

Eq. (5.2) can be rewritten

$$\frac{a^2}{a_f^2} = 1 + \frac{a_L^2}{a_f^2} + \frac{a_T^2}{a_f^2} \tag{5.3}$$

or

$$\frac{a_f^2}{a^2} = \frac{1}{1 + \frac{a_L^2}{a_f^2} + \frac{a_T^2}{a_f^2}} \tag{5.4}$$

The flexural, longitudinal and torsional wave energy per unit area and per unit of time are respectively

$$I_f = \rho c_f \frac{a_f^2}{\omega^2} \tag{5.5}$$

$$I_L = \rho c_L \frac{a_L^2}{\omega^2} \tag{5.6}$$

$$I_T = \rho c_T \frac{a_T^2}{\omega^2} \tag{5.7}$$

where ρ is the density of the material, ω the frequency, c_f, c_L and c_T the flexural, longitudinal and torsional wave speeds respectively.

The assumption of equi-partition of energy means that

$$I_f = I_L = I_T \tag{5.8}$$

or

$$c_f a_f^2 = c_L a_L^2 = c_T a_T^2 \tag{5.9}$$

Using Eq (5.9) and (5.10), and making the assumption that the different wave speeds are constant in a given frequency band, we have

$$\frac{a_f^2}{a^2} = \frac{1}{1 + \frac{c_f^2}{c_L^2} + \frac{c_f^2}{c_T^2}} \tag{5.10}$$

Following the same process, this can be calculated for longitudinal and torsional waves

$$\frac{a_L^2}{a^2} = \frac{1}{1 + \frac{c_L^2}{c_f^2} + \frac{c_L^2}{c_T^2}} \tag{5.11}$$

$$\frac{a_T^2}{a^2} = \frac{1}{1 + \frac{c_T^2}{c_f^2} + \frac{c_T^2}{c_L^2}} \tag{5.12}$$

The following table provides the values of these coefficients in different octave bands.

	c_f	c_L	c_T	$\frac{a_f^2}{a^2}$	$\frac{a_L^2}{a^2}$	$\frac{a_T^2}{a^2}$
125	126	5050	3115	0.938	0.023	0.038
250	178	5050	3115	0.915	0.032	0.052
500	251	5050	3115	0.884	0.044	0.072
1000	356	5050	3115	0.844	0.059	0.097
2000	503	5050	3115	0.793	0.079	0.128

Table 5.1: Partition coefficients of acceleration using equi-partition of energy.

Now taking into account the partition of acceleration previously calculated, the total axial antilog attenuation along the truss is given by

$$B^2_{\text{oct. band}} = \frac{a_f^2}{a^2} B^2_{\text{f, oct. band}} + \frac{a_L^2}{a^2} B^2_{\text{L, oct. band}} + \frac{a_T^2}{a^2} B^2_{\text{T, oct. band}} \tag{5.13}$$

The resulting step function is plotted in Fig 5.5.

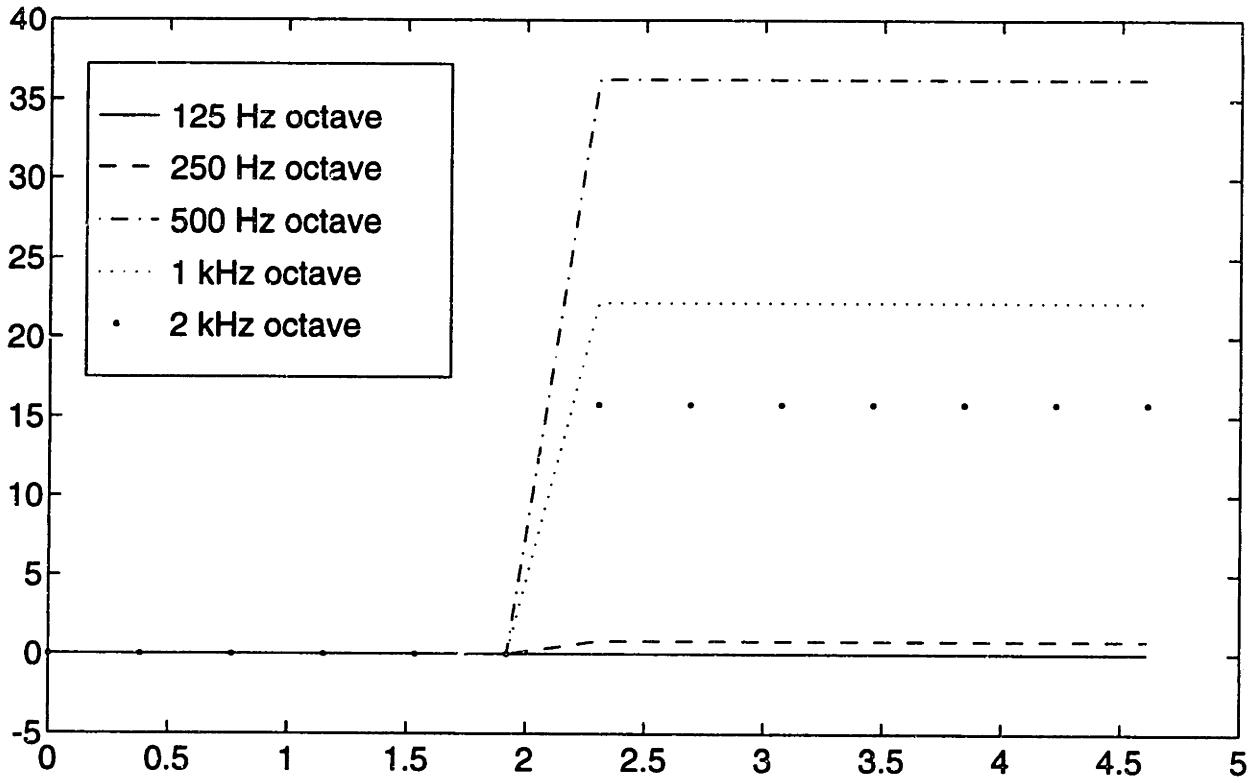

Figure 5.5: Predicted axial attenuation along the truss using equi-partition of energy

These curves deviate significantly from the experimental data (see Figs. 5.1 and 5.2). The predicted step function in the treated area is much larger, especially for the 500 Hz octave bands. At least one of the assumption made to build the predicted attenuation is invalid.

The transfer function between the rods and the joints varies among different wave types and may prevent accurate measurement of the attenuation on the rods when measuring the level of vibration at the joints. However an attenuation of 40 dB on the rods which results in an attenuation of only 5 dB on the second half of the truss is not realistic. So the assumption of equi-partition of energy is probably incorrect, especially at low frequencies. This is the first indirect evidence that energy in the truss is not equally partitioned among different wave types.

A more realistic partitioning is proposed. Assume instead that each wave type accounts for one third of the total *acceleration.*, so that

$$B^2_{\text{oct. band}} = B^2_{\text{f, oct. band}} + B^2_{\text{L, oct. band}} + B^2_{\text{T, oct. band}} \qquad (5.14)$$

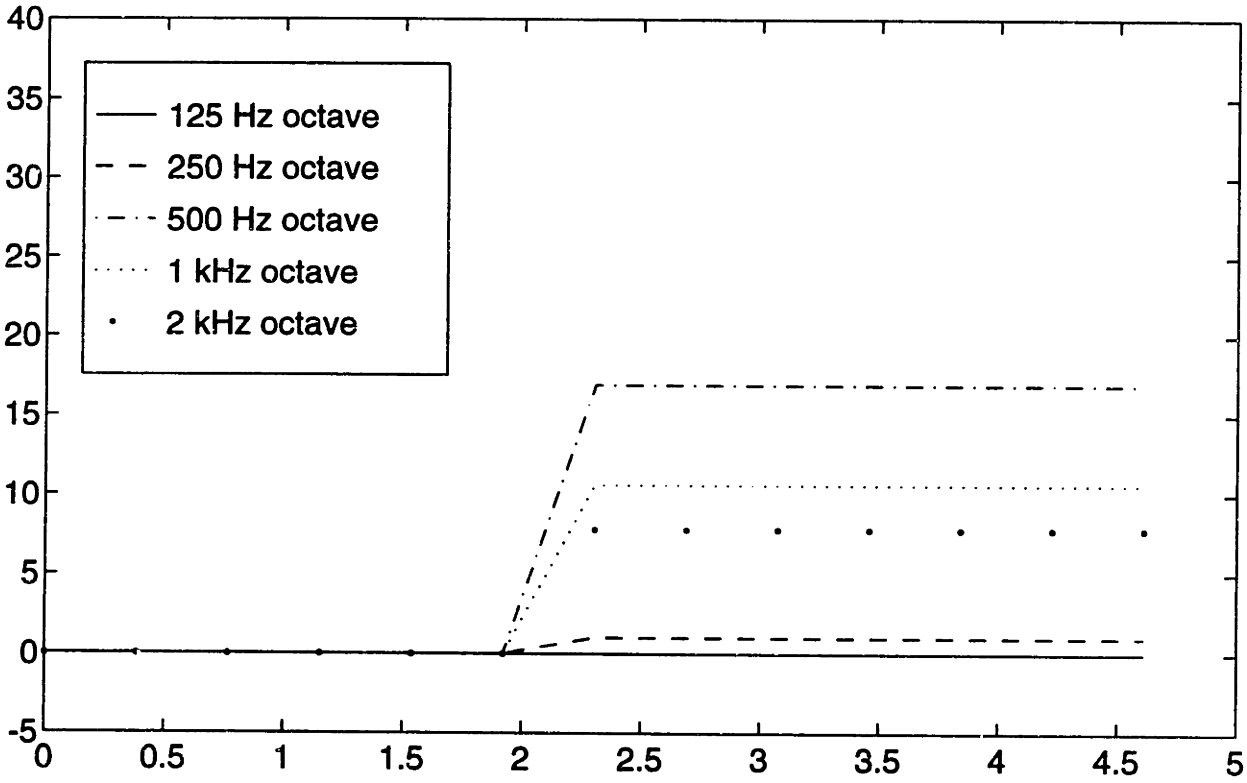

Figure 5.6: Predicted axial attenuation along the truss using equi-partition of accelerance

The resulting curve is plotted on Fig. 5.6. This prediction fits better with the experimental data, although the step function in the 500 Hz octave band is too large.

This higher level of predicted attenuation questions the validity of considering only right-travelling waves. This case is considered because the models described in Chapter 2 are developed for right-going waves travelling on semi-infinite rod. In fact, waves are reflected at each end of the truss and travel back and forth. In the next section, a new theory is derived to take this phenomenon into account.

Furthermore, the analytical model is based on the continuity criterion of the layer of dynamic absorbers. For flexural waves, this criterion is no longer valid above 1200 Hz. So

at high frequencies, other mechanism of attenuation may be involved. A description of the mechanisms involved is proposed in Section 5.5.

5.3 Analytical Model for a Finite Rod with a Dynamic Absorber Layer

In this section, a new analytical model is introduced to describe the attenuation of waves on a *finite* rod loaded with a layer of dynamic absorbers. The process is similar for any wave type, so we consider that the wave number k can either be the flexural, longitudinal or torsional wavenumber. The values of these wavenumbers are given in Chapter 2.

In a semi-infinite rod with a dynamic absorber layer, the attenuation of propagating waves is a linear function of the distance and is given by

$$A(x) = 20 \log(e^{k_i x}) = 8.69 k_i x \text{ , in dB per distance x} \qquad (5.15)$$

where k_i is the imaginary part of the wave number and x is the axial distance along the rod.

Now consider a finite tube.

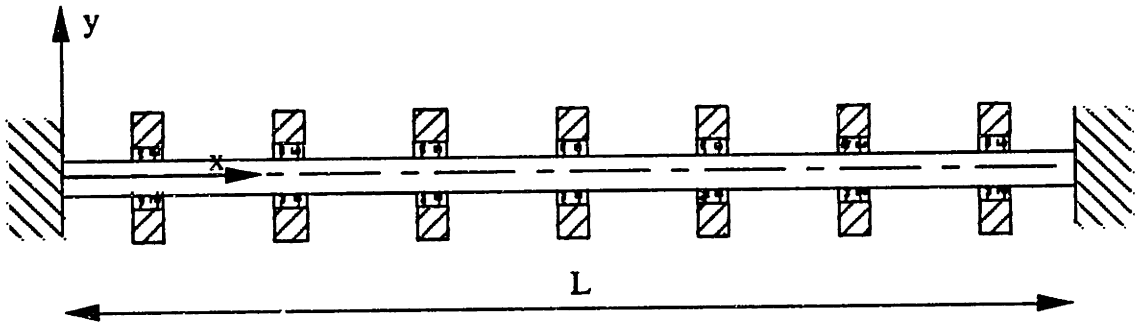

Figure 5.7: Finite beam with a layer of dynamic absorbers.

Suppose that a wave in the form $e^{(ikx-i\omega t)}$ starts at x=0. This wave is travelling in the +x direction and is attenuated by the layer of dynamic absorbers. At x=L, the attenuation is the magnitude of e^{ikL}. We make the assumption that this wave is perfectly reflected and travels back in the beam. The reflected wave is in the form $e^{ikL}\, e^{-ik(x-L)-i\omega t}$. At x=0 we also make the assumption that the left-going wave is perfectly reflected.

The displacement of the rod, u_1, is then the addition of an infinite number of right and left travelling waves. So we have

$$u_1(x)_{finite} = Ue^{ikx} + Ue^{ikL}\, e^{-ik(x-L)} + Ue^{2ikL}\, e^{ikx} + e^{3ikL}\, e^{-ik(x-L)} + \ldots$$

where $U = U_0\, e^{-i\omega t}$

$$u_1(x)_{finite} = \sum_{p=o} Ue^{2pikL}\, e^{ikx} + \sum_{q=o} Ue^{(2q+1)ikL}\, e^{-ik(x-L)} \qquad (5.16)$$

These two terms are the sums of geometric series

$$u_1(x)_{finite} = U\frac{1}{1-e^{2ikL}}\, e^{ikx} + U\frac{e^{ikL}}{1-e^{2ikL}}\, e^{-ik(x-L)} \qquad (5.17)$$

With some manipulation we find that

$$u_1(x)_{finite} = U\,\frac{e^{ik(x-L)} + e^{-ik(x-L)}}{e^{-ikL} - e^{ikL}} \qquad (5.18)$$

The magnitude of this complex number gives the attenuation along the tube.
In dB we have

$$A(x)_{finite} = -20 \log\left[\text{mag}\left(\frac{e^{ik(x-L)} + e^{-ik(x-L)}}{e^{-ikL} - e^{ikL}}\right)\right] \qquad (5.19)$$

The attenuation versus distance is plotted at different frequencies in Fig. 5.8, 5.9, 5.10 and 5.11. The resonance frequency of the dynamic absorbers is 450 Hz and the mass ratio is 3. The length of the beam is 0.5 m. The attenuation obtained is compared to the equivalent linear attenuation due to an infinite rod. Notice that the attenuation at a distance equal to L is less in the finite case.

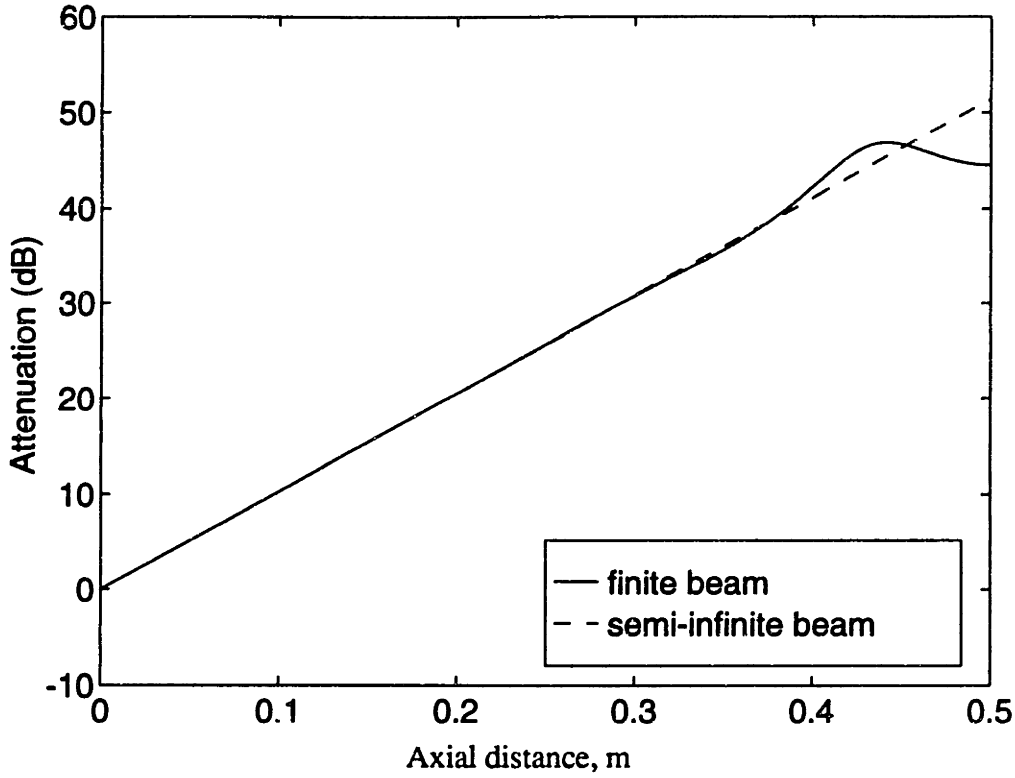

Figure 5.8: Flexural attenuation for a finite beam at 500 Hz.

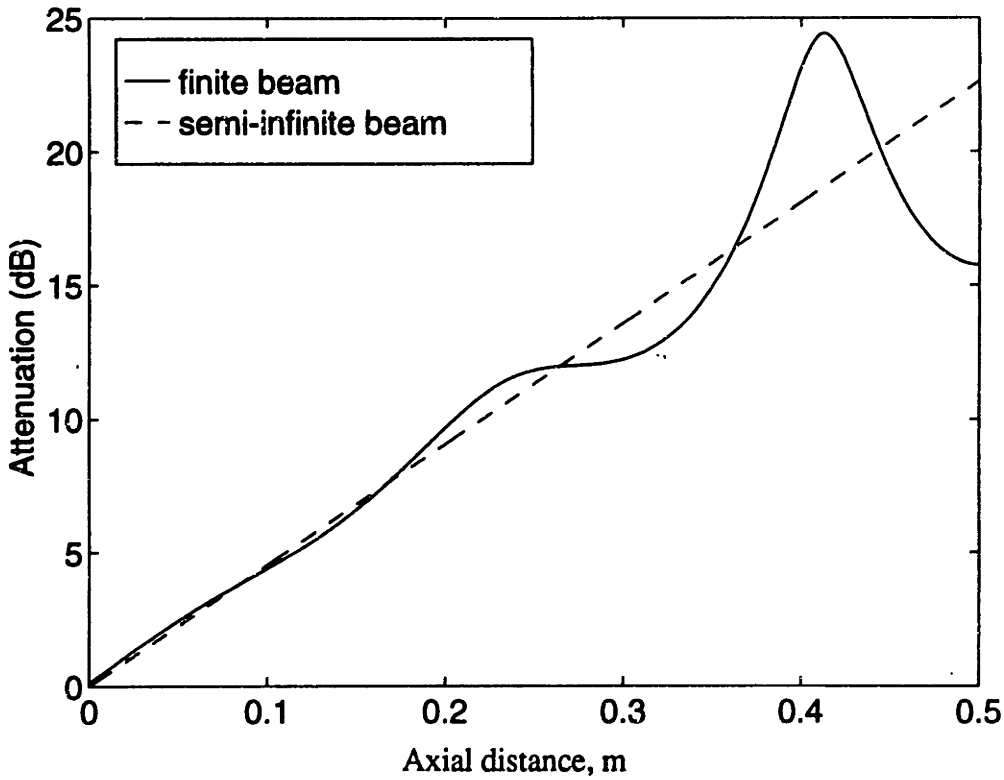

Figure 5.9: Flexural attenuation for a finite beam at 1000 Hz.

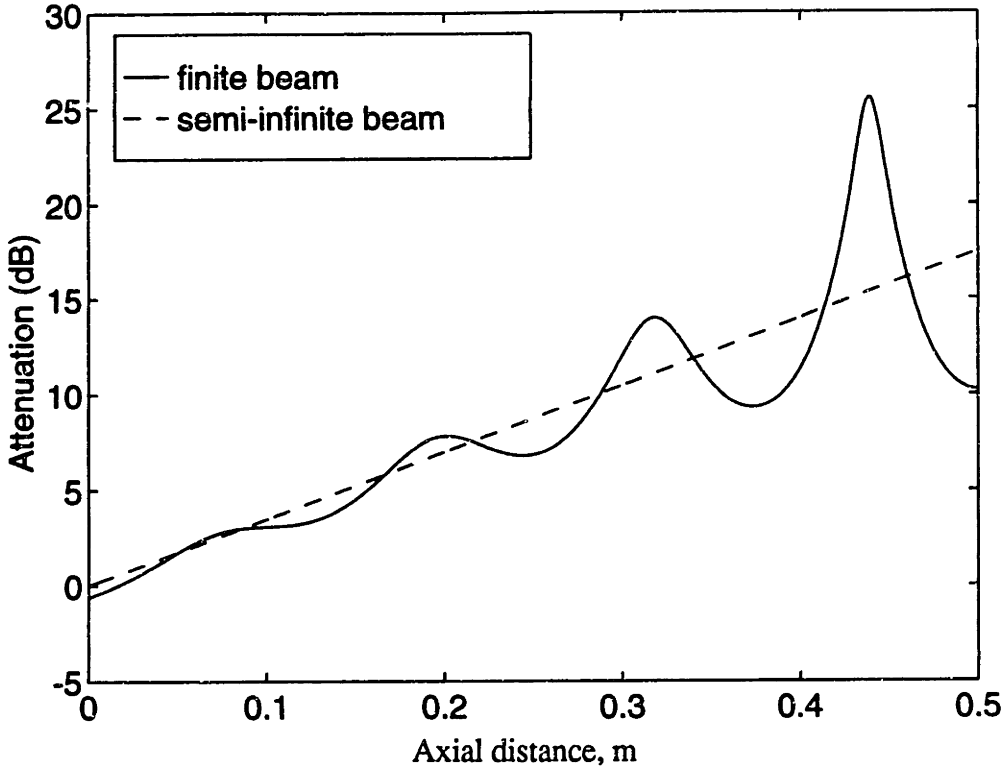

Figure 5.10: Flexural attenuation for a finite beam at 2000 Hz.

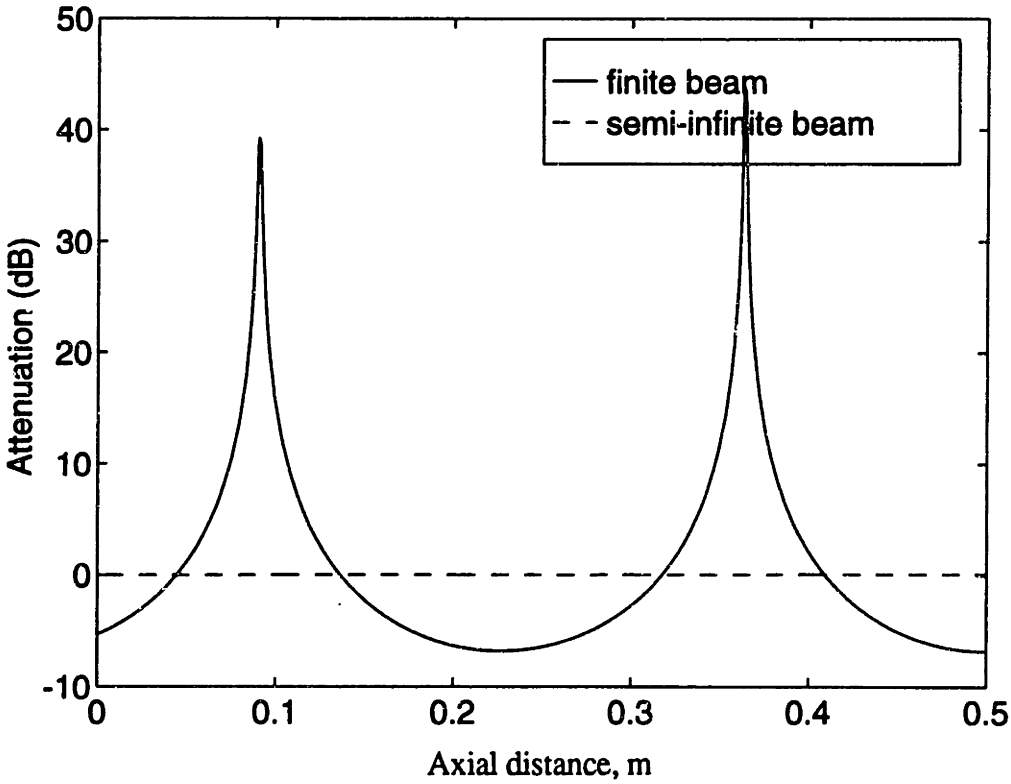

Figure 5.11: Flexural attenuation for a finite beam at 200 Hz.

5.4 Experimental Validation of the New Analytical Model

An experiment has been conducted to validate the finite loaded rod analytical model. The configuration of the truss is 'fully damped' (Chapter 4). We consider a rod located in the treated area of the truss. The rod chosen is 50 cm long and crosses the treated area. A total of six dynamic absorbers are on this rod, one every 7.3 cm. A shaker is attached to one end of the rod. The shaker is perpendicular to the axis of the rod, so that flexural waves are highly excited. The setup is presented on Fig 5.12 .

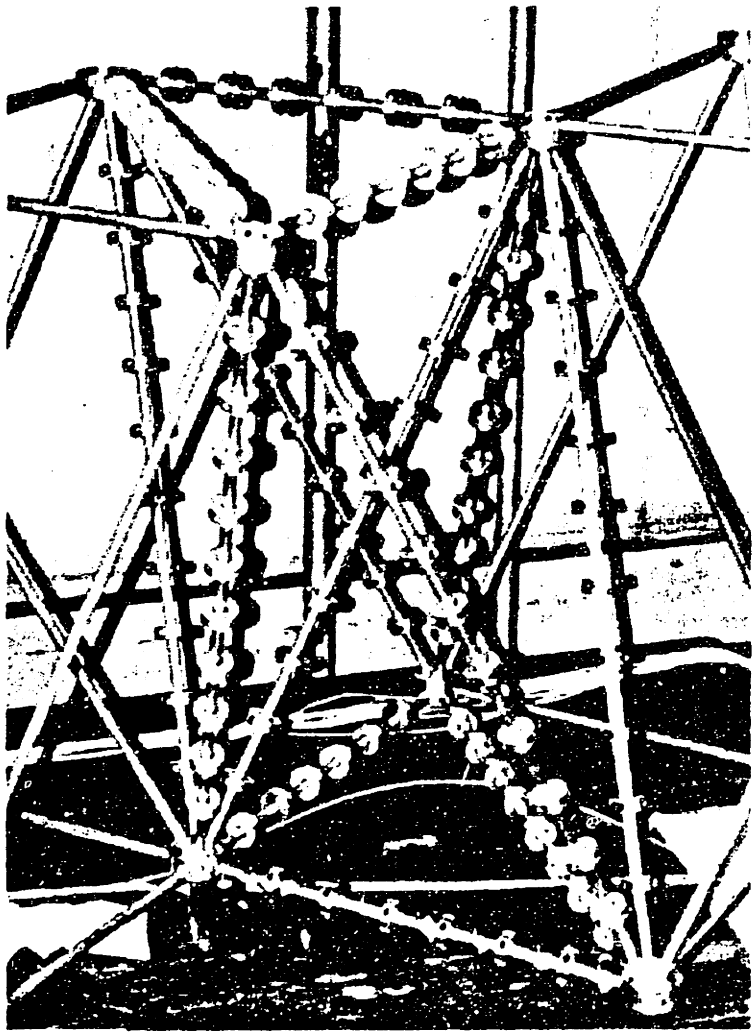

Figure 5.12: Photograph of the experimental test of attenuation for a finite beam.

Seven PCB model 309A accelerometers are placed on the rod between dynamic absorbers. They are oriented in a direction normal to the main axis of the rod and are attached with bees wax. They are numerated from one to seven as shown in Fig 5.13.

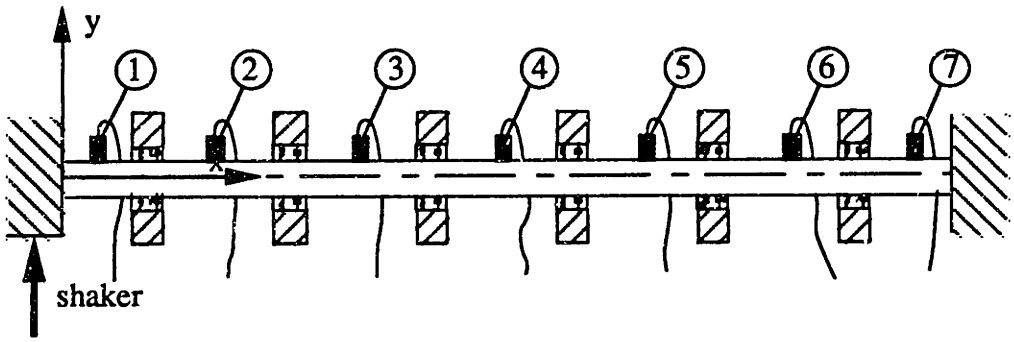

Figure 5.13: setup and enumeration of the accelerometers for the validation test

An HP 3562A two channel dynamic analyzer is used in the same configuration as the single resonance frequency test described in Chapter 3. The input is band limited white noise. The transfer function between the accelerance measured at accelerometer 1 and the six other accelerometers is plotted.

Three of these curves corresponding to the transfer functions between 2 and 1, 4 and 1, 7 and 1, are presented respectively in Figs. 5.14, 5.15 and 5.16. They are compared with the equivalent analytical predictions. The infinite rod model is plotted with dotted line, the new analytical model is plotted with a continuous line.

Both curves agree with the experimental data, but the new analytical model is more refined. At low frequencies, it takes into account peaks observed on the experimental curve, corresponding to resonance frequencies of the rod. At the end of the rod (accelerometer 7) the behavior is better described. The infinite model, which does not take into account waves coming back, overestimates the level of attenuation by 10 dB at high frequencies. The finite model corrects this overestimation and fits with the experimental curve.

In conclusion this experiment proves that:

- the new finite model better describes phenomena involved in finite rods than the semi-infinite rod model,
- the mechanism of attenuation due to a layer of dynamic absorbers is actually taking place in the truss as predicted (except for the higher frequencies at which the spacing criterion of the analytical models is violated; see section 5.5).

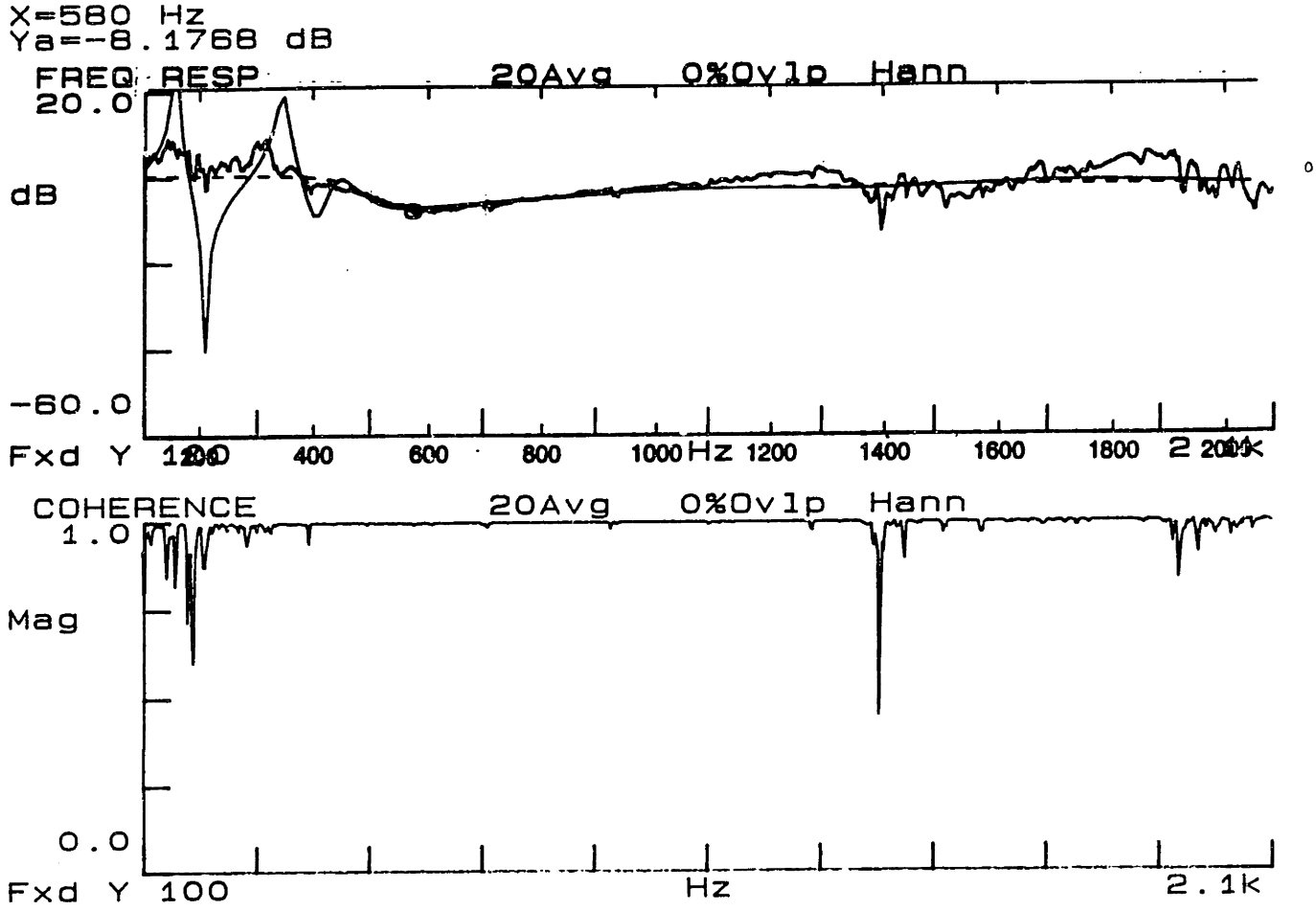

Figure 5.14: Transfer function between accelerometer 2 and accelerometer 1.

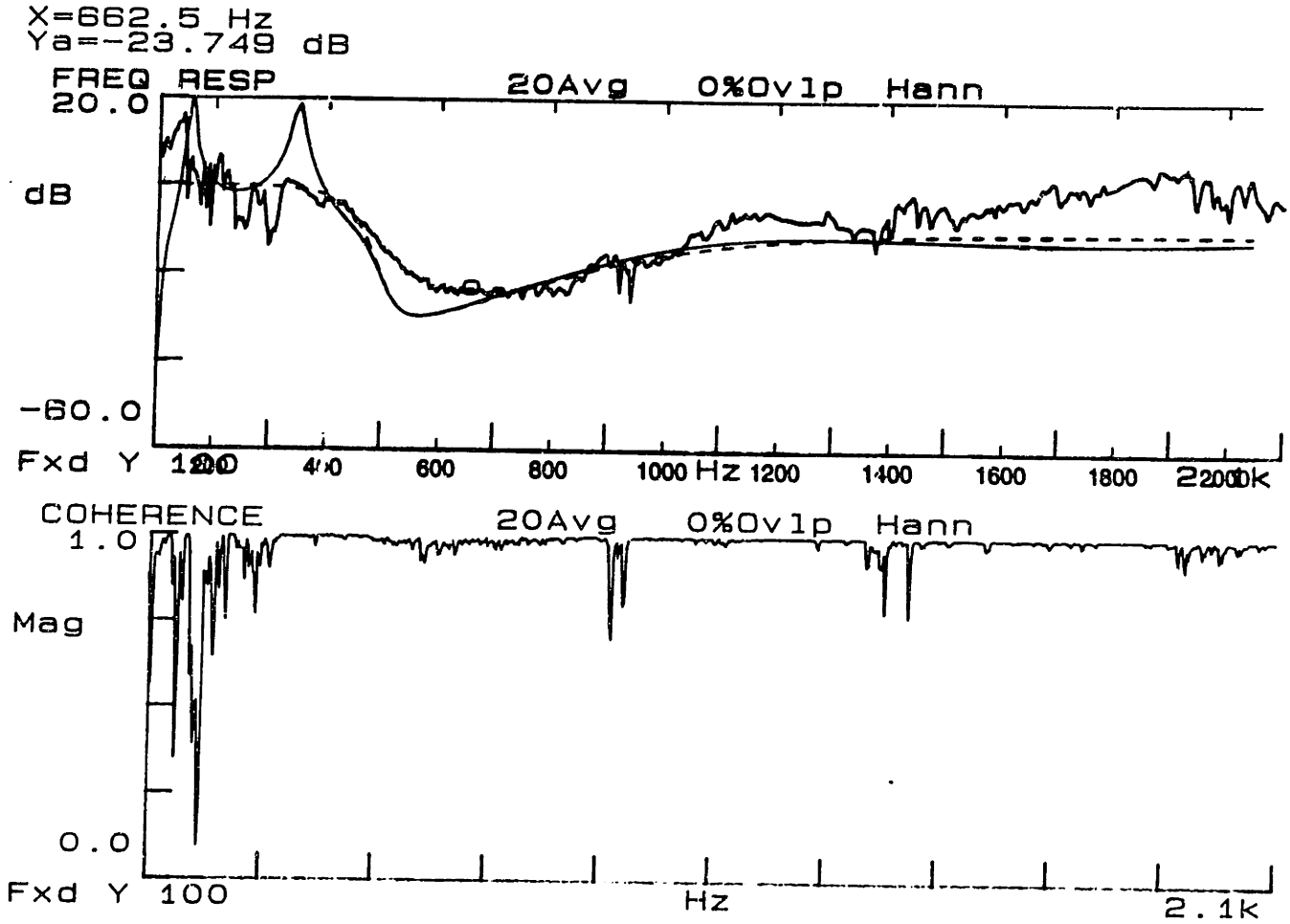

Figure 5.15: Transfer function between accelerometer 4 and accelerometer 1.

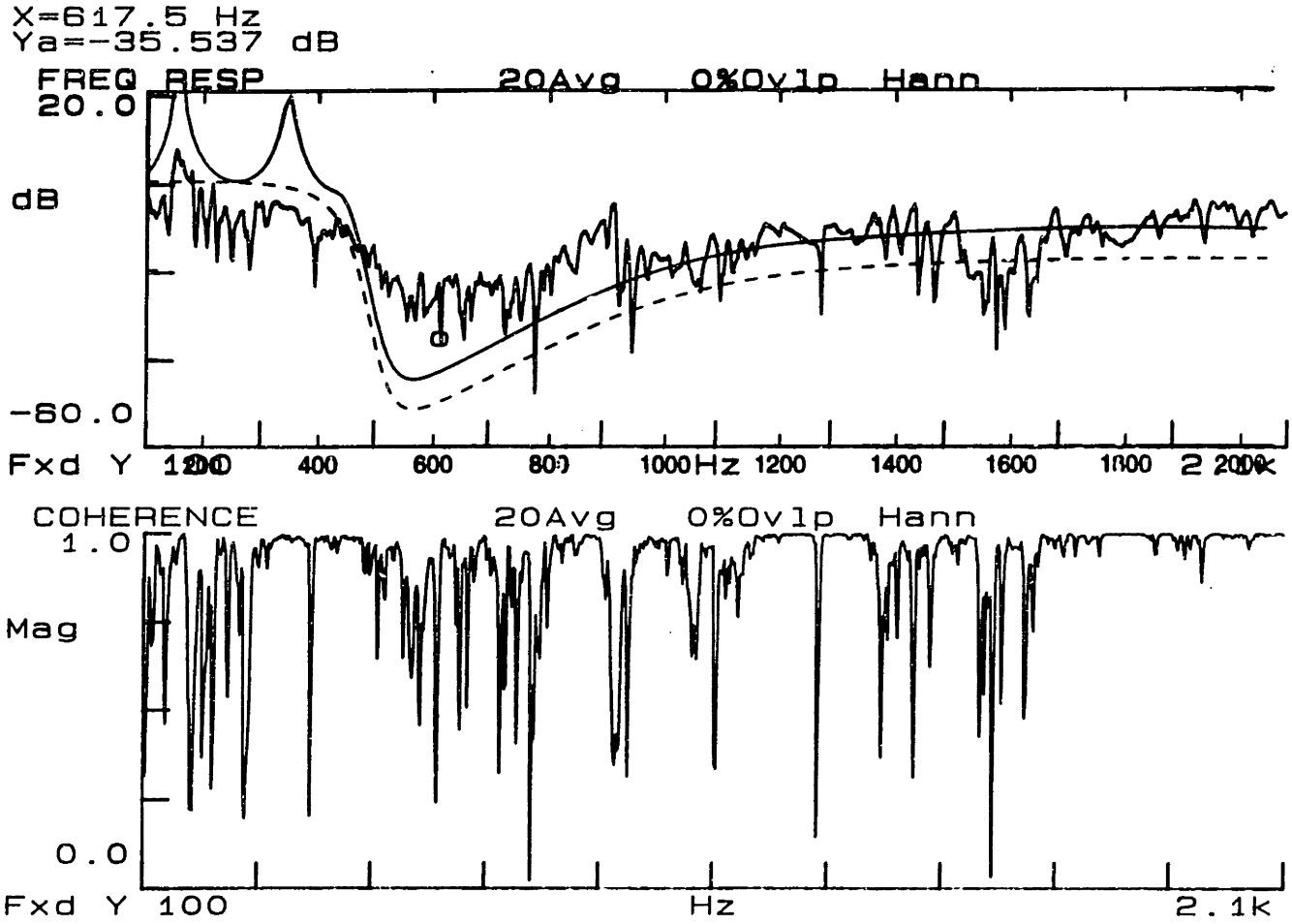

Figure 5.16: Transfer function between accelerometer 7 and accelerometer 1.

5.5 Behavior of a Layer of Dynamic absorbers at High Frequencies

To understand the mechanism involved at high frequencies, I make the assumption that the wavelength of the propagating waves is no longer larger than the spacing of the dynamic absorbers, but still larger than the width of the attached masses. Under such conditions, the dynamic absorbers act as "blocking springs". The difference in impedance between the loaded and unloaded part is responsible for the reflection of the waves.

In the following section, I do not intend to do more than introducing the nature of the ensuing complexities with a few preliminary calculations for their full exposition would be beyond the scope of this thesis.

First, the reflection coefficient due to one dynamic absorber is calculated for longitudinal waves. The same computation can be conducted for flexural waves, although the formulation is much more complicated. The calculation for flexural waves can be derived from a "blocking mass" study [9], but as the physical ideas for all wave types are well embodied by the longitudinal case, only the longitudinal case is considered. After this first step, a process is proposed to evaluate a global transmission coefficient due to the effect of the periodic spacing of the absorbers.

Single transmission coefficient for longitudinal waves

Consider a dynamic absorber located on an infinite rod. The velocities v_1 and v_3 on the two sides of the mass are equal, and the resultant velocity ahead of the mass may be considered as composed of an incoming and of a reflected part, as shown in Fig 5.17.

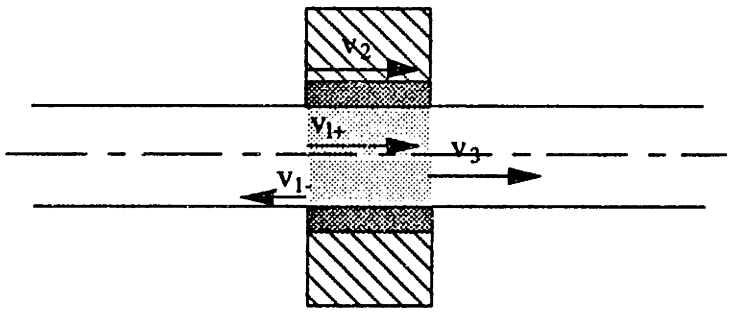

Figure 5.17: Dynamic absorber on an infinite rod.

$$v_1 = v_{1+} + v_{1-} = v_3 \tag{5.20}$$

However, the force acting on the two sides of the mass are different, and their difference accelerates the mass through the resilient layer. The difference between F_1 and F_3 , F, can be found by solving the equations of motion for the mass and the rod

$$R_L\frac{\partial}{\partial t}(v_3-v_2) + k_L(v_3-v_2) = F \tag{5.21}$$

$$m\frac{\partial^2 v_2}{\partial t^2} + R_L\frac{\partial}{\partial t}(v_2-v_3) + k_L(v_2-v_3) = 0 \tag{5.22}$$

Consider harmonic displacements of the form exp(ikx -iωt). We have

$$-i\omega R_L(v_3-v_2) + k_L(v_3-v_2) = F \tag{5.23}$$

$$-i\omega^2 m v_2 - i\omega R_L(v_2-v_3) + k_L(v_2-v_3) = 0 \tag{5.24}$$

Eq. (5.23) gives

$$v_2 = \frac{k_L - i\omega R_L}{-i\omega^2 m - i\omega R_L + k_L} v_3 \tag{5.25}$$

and using Eq. (5.24), one finds

$$F = -i\omega^2 m \frac{k_L - i\omega R_L}{-i\omega^2 m - i\omega R_L + k_L} v_3 \tag{5.26}$$

Notice that for low frequencies, $F = -i\omega^2 m v_3$; the dynamic absorber acts like a "blocking mass". For high frequencies (large compared to the the resonance frequency of the dynamic absorber), $F= (k_L - i\omega R_L)v_3$; for small values of the resistance, the dynamic absorber acts like a "blocking spring".

The resultant force acting on the front of the mass can also be considered as made up of an incident and a reflected part and these components are proportional to the corresponding displacement components, v_{1+} and v_{1-}.

$$F_{1+} = i\omega Z_1 v_{1+} \tag{5.27}$$

$$F_{1-} = i\omega Z_1 v_{1-} \tag{5.28}$$

where Z_1 is the impedance of the rod.

By substituting (5.27) and (5.28) into (5.26) one obtains

$$v_{1+} - v_{1-} = v_3\left(1 + \frac{-i\omega^2 m\,(k_L - i\omega R_L)}{-i\omega^2 m - i\omega R_L + k_L}\,\frac{1}{Z_1}\right) \tag{5.29}$$

and by use of (5.8) one finds the transmission coefficient

$$\tau = \frac{v_3}{v_{1+}} = \frac{1}{1 + \dfrac{-i\omega^2 m\,(k_L - i\omega R_L)}{-i\omega^2 m - i\omega R_L + k_L}\,\dfrac{1}{2Z_1}} \tag{5.30}$$

The reflection coefficient is given by the relation

$$\tau^2 + \mathcal{R}^2 = 1 \tag{5.31}$$

Global reflection coefficient

The treated rods considered in the experiment possess many equally spaced dynamic absorbers. As a reflection coefficient is introduced at each attached mass, waves travel back and forth before reaching the end of the rod. This configuration can be compared to the propagation of waves travelling in changing continuous media, a topic largely covered in [10].

First consider two identical dynamic absorbers which separate a rod into three continuous parts.

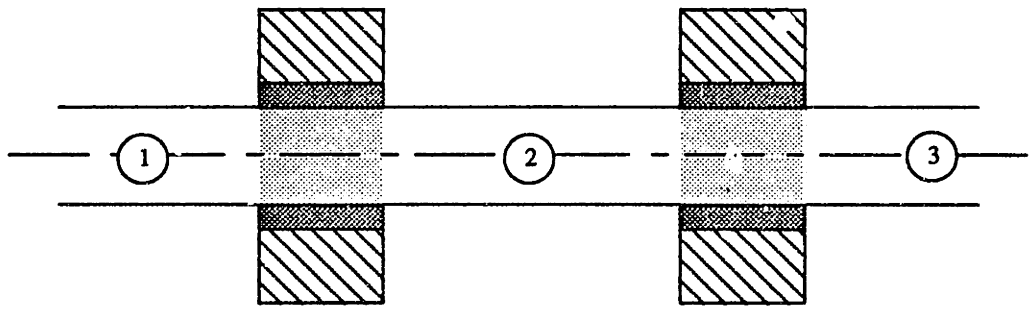

Figure 5.18: Two dynamic absorbers on an infinite rod.

The reflection coefficient between 1 and 3, $\mathcal{R}_{13}$, is given by

$$\mathcal{R}_{13} = \frac{\mathcal{R}_{23} + \mathcal{R}_{12}\, e^{2ikd}}{1 + \mathcal{R}_{23}\mathcal{R}_{12}\, e^{2ikd}} \tag{5.32}$$

where d is the spacing of the absorbers.

In that case, the local reflection coefficients are the same so that we have

$$\mathcal{R}_{13} = \frac{\mathcal{R} + \mathcal{R}\, e^{2ikd}}{1 + \mathcal{R}^2\, e^{2ikd}} \tag{5.33}$$

By recurrence it is possible to extend the previous formula to n parts (n-1 dynamic absorbers), and obtain a global reflection coefficient.

The single coefficients, and therefore the global ones, are highly frequency dependent. In the experiment described in chapter 4, the axial attenuation is considered for octave bands only. A full theory for n-1 dynamic absorbers would be very difficult to compare. The aim of the preliminary calculations is not to corroborate experiment but rather to suggest a mechanism for the phenomena involved at high frequencies where a step function located in the dynamic absorbers area subsists above 1 kHz in the experimental data.

6 Conclusion

An experiment has been conducted to show the attenuation caused by the addition of dynamic absorbers on a truss. Rods located in the middle of the truss have been treated so that no wave can propagate from one end to the other without going through a loaded rod. The steady state attenuation of acceleration as a function of axial distance is measured for the damped and undamped truss and plotted for different octave bands. The difference between the damped and undamped curves shows the effect of the dynamic absorbers.

The overall shape of the differential curves of attenuation versus axial distance is a step function, with the step located in the dynamic absorbers attachment area. The step is dramatic for frequency bands ranging from the 250 Hz octave band to the 4 kHz octave band. For low frequencies, the attenuation due to dynamic absorbers is not significant. At high frequencies the attenuation level is higher than expected all along the truss. The main effect of the dynamic absorbers is to separate the truss in two parts with two different levels of vibration.

Assuming the equi-partition of energy between the different wave types and using the classical theory of attenuation of waves propagating on a semi-infinite rod loaded with a continuous layer of dynamic absorbers, one can predict the axial attenuation along the truss. The assumption of equi-partition of energy proves to be incorrect. The equi-partition of acceleration is a better assumption but the level of attenuation predicted is still too high. The applicability of the semi-infinite model is questioned by these results. As a consequence, a refinement of the model has been constructed to take into account the finite boundary conditions of the rods used in the truss. This model has been validated by an experiment and better estimates the attenuation at the end of each treated rod.

An explanation is proposed for the existence of the experimental step function at higher frequencies in the treated area. For flexural waves, the assumption of continuity is no longer valid above 1200 Hz. In such conditions, the dynamic absorber act as a "blocking spring". The difference in impedance between the loaded and unloaded part is responsible for the reflection of waves. Meanwhile, for this range of frequencies, attenuation of torsional and longitudinal waves are still expected to be predicted by continuous dynamic absorbers models.

No explanation is proposed for the existence of a step function near the source of excitation at high frequencies.

This study proves that the use of dynamic absorbers applied in a local region is a potential treatment for especially noisy source regions or especially sensitive mounting areas.

The behavior of dynamic absorbers at frequencies for which the continuity assumption is no longer valid has been studied for longitudinal waves. Future work should validate this theory by measuring the reflection coefficient of a single loaded rod supporting longitudinal waves. An analytical model should also be derived and validated for the reflection of flexural waves. The calculation can be derived from the theory of blocking masses found in [9].

The knowledge of the steady state energy balance between the different kinds of waves is essential to predict exactly the level of axial attenuation along the truss. The assumption of equi-partition of energy has been proposed, but the predicted attenuation following this assumption does not fit with experimental data. The equi-partition of acceleration is a more realistic assumption. Future work should focus on the determination of the partitioning between the different wave types.

References

[1] Marcus R. A. Heath, "Dynamic Behavior of a Three Dimensional Aluminium Truss in Free Space", S.M. Thesis, Massachusetts Institute of Technology, 1994.

[2] Timothy L. Smith, Kodali Rao, Ira Dyer, "Attenuation of Plate Flexural Waves by a Layer of Dynamic Absorbers", *Noise Control Engineering Journal*, April 1986.

[3] Kevin LePage, "The Attenuation of Flexural Waves in Assymetrically Mass Loaded Beams", S.M. Thesis, Massachusetts Institute of Technology, 1986.

[4] Lawrence Olivieri, "The Effect of Dynamic Absorbers on Longitudinal wave Propagation in a Circular Rod", S.M. Thesis, Massachusetts Institute of Technology, 1989.

[5] Charles Corrado, Rebecca Zavistoski, Ira Dyer, "Coupled Wave Complexity in Structural Acoustics", *The American Society of Mechanical Engineers*, Dallas, November 1990.

[6] Charles E. Crede, Vibration and Shock Isolation, John Wiley & Sons, New York, 1951.

[7] Richard E. Sapienza, "Wave Propagation Symetry in a rod with a Dynamic Absorber Layer", S.M. Thesis, Massachusetts Institute of Technology, 1992.

[8] William W. Seto, Theory and Problems of Mechanical Vibration, McGraw-Hill Book Company, 1964.

[9] Cremer, Heckl, Ungar, Structure-Borne Sound, second edition, Springer-Verlag, 1973.

[10] Brekhovsky, Lysanov, Fundamentals of Ocean Acoustics, second edition, Springer-verlag, 1982.

Appendix A: Matlab Codes for Calculation of Various Graphs.

Figures 2.2 and 2.3: Attenuation of flexural waves on a rod loaded with a continuous distribution of dynamic absorbers.

```
clear
clf
%
%plot flexural attenuation on a rod due to a continuous distribution of abs.
%
beta=3;
wo=450*2*pi;
%
x=0:0.02:3;
%
y=1./x;
kf=sqrt((x.*wo)./(0.004*5096));
%
nu=0.01;
kif=kf.*imag((1+beta*(nu+i.*y.*y)./(nu+i.*y.*y-i)).^(0.25));
Af1=8.686*kif;
%
nu=0.1;
kif=kf.*imag((1+beta*(nu+i.*y.*y)./(nu+i.*y.*y-i)).^(0.25));
Af2=8.686*kif;
%
nu=0.3;
kif=kf.*imag((1+beta*(nu+i.*y.*y)./(nu+i.*y.*y-i)).^(0.25));
Af3=8.686*kif;
%
nu=0.5;
kif=kf.*imag((1+beta*(nu+i.*y.*y)./(nu+i.*y.*y-i)).^(0.25));
Af4=8.686*kif;
%
axes('position',[0.2,0.2,0.56,0.56]);
plot(x,Af1,':');
hold on;
plot(x,Af2,'-.');
plot(x,Af3,'--');
plot(x,Af4,'-');
ylabel('dB')
%title('Predicted flexural Attenuation per meter, as a function frequency normalized by the oscillator flexural resonance frequency ')

legend('0.01','0.1','0.3','0.5')
```

Figures 2.5 and 2.6: Attenuation of longitudinal waves on a rod loaded with a continuous distribution of dynamic absorbers.

```
clear
clf
%
%plot longitudinal attenuation on a rod due to a continuous distribution of abs.
%
beta=3;
wo=450*2*pi;
%
x=0:0.02:3;
w=x.*wo;
kl=w./5091;
%
nu=0.01;
kil=kl.*imag((1+beta.*(1-i.*nu.*x)./(1-i.*nu.*x-x.*x)).^(0.5));
Al1=8.686*kil;
%
nu=0.1;
kil=kl.*imag((1+beta.*(1-i.*nu.*x)./(1-i.*nu.*x-x.*x)).^(0.5));
Al2=8.686*kil;
%
nu=0.3;
kil=kl.*imag((1+beta.*(1-i.*nu.*x)./(1-i.*nu.*x-x.*x)).^(0.5));
Al3=8.686*kil;
%
nu=0.5;
kil=kl.*imag((1+beta.*(1-i.*nu.*x)./(1-i.*nu.*x-x.*x)).^(0.5));
Al4=8.686*kil;
%
%
axes('position',[0.2,0.2,0.56,0.56]);
plot(x,Al1,':',x,Al2,'-.',x,Al3,'--',x,Al4,'-');
%xlabel('Normalized Frequency')

ylabel('dB ')

%title('Predicted longitudinal attenuation per meter, as a function frequency normalized by the oscillator longitudinal resonance frequency ')

legend('0.01','0.1','0.3','0.5')
```

Figures 4.5 and 4.6: Difference of attenuation versus axial distance between the half damped and the undamped configuration

```
clear
clf
% enter raw data

% ie.  a2   a4   a6   a8   a10   a12
a125=[-11.98 -15.88 -15.64 -17.3 -18.29 -8.14];
a250=[-6.44 -10.14 -11.57 -12.21 -9.68 -7.56];
a5=[-.42 -1.52 -.1 -1.65 -3 -2.13];
a1=[4.32 2.05 2.54 2.48 1.58 1.85];
a2=[3.64 .05 .27 -2.06 -2.21 -1.4];
a4=[5.27 -1.38 -5.56 -8.28 -9.37 -11.22];
a8=[7.59 -2.65 -6.55 -11.35 -13.07 -13.56];
a16=[2.03 -3.22 -9.57 -15.08 -19.69 -25.39];
a3=[-.62 -3.42 -7.18 -12.18 -19.06 -25.28];
b125=[-10.11 -17.52 -14.83 -15.41 -16.78 -12.67 -8.73];
b250=[-5.92 -9.32 -11.13 -12.57 -12.71 -13.72 -7.37];
b5=[2.78 -2.2 -1.66 .03 -1.46 -3.66 1.62];
b1=[8.32 3.26 2.67 2.11 1.62 1.63 2.19];
b2=[6.70 7.56 3.97 2.46 -.73 1.43 -2.21];
b4=[9.37 3.39 -1.15 -5.01 -9.32 -9.47 -13.1];
b8=[13.70 7.71 -5.36 -9.04 -14.79 -15.95 -25.14];
b16=[9.41 5.28 -5.05 -12.46 -17.08 -21.96 -26.43];
b3=[1.24 -.77 -5.61 -9.57 -15.82 -22.80 -26.37];
c125=[-15.53 -15.77 -14.36 -17.62 -11.97 -10.86];
c250=[-6.64 -10.04 -10.66 -11.25 -12.64 -8.81];
c5=[-.65 -1.39 .87 -1.13 -3.14 -2.38];
c1=[4.06 2.62 2.46 2.11 1.01 1.25];
c2=[4.31 1.57 .42 -2.15 -2.12 -2.65];
c4=[5.94 -.95 -4.69 -7.51 -9.91 -10.94];
c8=[7.96 -1.62 -7.76 -10.13 -13.65 -13.96];
c16=[2.21 -4.17 -11.81 -15.84 -18.92 -23.87];
c3=[-.21 -3.26 -6.02 -12.01 -17.48 -24.55];
d125=[-13 -12.44 -14 -21.43 -12.33];
d250=[-10.7 -12.13 -12.48 -13.38 -9.86];
d5=[.25 -3.36 -4.1 -1.65 -3.75];
d1=[3 3.43 1.84 2.1 -.32];
d2=[3.79 -.26 -.78 -1.02 -3.14];
d4=[-.17 -6.34 -8.02 -8.3 -10.5];
d8=[-1.97 -9.54 -12.63 -15.14 -17.86];
d16=[-3.26 -9.78 -16.92 -20.22 -24.54];
d3=[-2.31 -4.87 -10.44 -17.08 -23.35];
e125=[-11.52 -16.03 -15.96 -19.21 -15.78 -12.58];
e250=[-9.02 -14.15 -12.71 -12.91 -17.12 -6.34];
e5=[2.04 -1.79 -2.6 -2.58 -2.18 1.1];
e1=[6.66 3.98 4.41 1.28 0.76 2.22];
e2=[5.46 3.76 4.48 .76 1.45 1.02];
e4=[3.15 -.64 -2.26 -8.32 -8.5 -11.21];
```

```
e8=[6.72 -1.98 -11.16 -19.53 -17.5 -21.04];
e16=[1.48 -4.51 -9.71 -16.65 -20.21 -27.41];
e3=[-2.74 -2.49 -5.66 -12.55 -20.01 -25.01];
f125=[-10.25 -13.75 -14.4 -21.24 -12.54];
f250=[-10.3 -16.36 -11.31 -12.73 -8.61];
f5=[-.71 -3.81 -3.54 -2.07 -2.97];
f1=[3.17 3.16 1.75 2.23 .5];
f2=[1.61 -.54 -.56 -.55 -2.75];
f4=[-.62 -7.27 -6.83 -7.59 -11.56]
f8=[-1.92 -12.91 -11.57 -15.44 -19.64];
f16=[-4.62 -11.1 -15.94 -21.46 -25.72];
f3=[-1.75 -5.41 -10.19 -14.59 -23.66];

% average three joints per section (excluding end joints b1, b13)

v1125=b125(1);
v2125=(a125(1)+c125(1)+e125(1))/3;
v3125=(b125(2)+d125(1)+f125(1))/3;
v4125=(a125(2)+c125(2)+e125(2))/3;
v5125=(b125(3)+d125(2)+f125(2))/3;
v6125=(a125(3)+c125(3)+e125(3))/3;
v7125=(b125(4)+d125(3)+f125(3))/3;
v8125=(a125(4)+c125(4)+e125(4))/3;
v9125=(b125(5)+d125(4)+f125(4))/3;
v10125=(a125(5)+c125(5)+e125(5))/3;
v11125=(b125(6)+d125(5)+f125(5))/3;
v12125=(a125(6)+c125(6)+e125(6))/3;
v13125=b125(7);

v1250=b250(1);
v2250=(a250(1)+c250(1)+e250(1))/3;
v3250=(b250(2)+d250(1)+f250(1))/3;
v4250=(a250(2)+c250(2)+e250(2))/3;
v5250=(b250(3)+d250(2)+f250(2))/3;
v6250=(a250(3)+c250(3)+e250(3))/3;
v7250=(b250(4)+d250(3)+f250(3))/3
v8250=(a250(4)+c250(4)+e250(4))/3;
v9250=(b250(5)+d250(4)+f250(4))/3;
v10250=(a250(5)+c250(5)+e250(5))/3;
v11250=(b250(6)+d250(5)+f250(5))/3;
v12250=(a250(6)+c250(6)+e250(6))/3;
v13250=b250(7);

v15=b5(1);
v25=(a5(1)+c5(1)+e5(1))/3;
v35=(b5(2)+d5(1)+f5(1))/3;
v45=(a5(2)+c5(2)+e5(2))/3;
v55=(b5(3)+d5(2)+f5(2))/3;
v65=(a5(3)+c5(3)+e5(3))/3;
v75=(b5(4)+d5(3)+f5(3))/3;
v85=(a5(4)+c5(4)+e5(4))/3;
```

```
v95=(b5(5)+d5(4)+f5(4))/3;
v105=(a5(5)+c5(5)+e5(5))/3;
v115=(b5(6)+d5(5)+f5(5))/3;
v125=(a5(6)+c5(6)+e5(6))/3;
v135=b5(7);

v11=b1(1);
v21=(a1(1)+c1(1)+e1(1))/3;
v31=(b1(2)+d1(1)+f1(1))/3;
v41=(a1(2)+c1(2)+e1(2))/3;
v51=(b1(3)+d1(2)+f1(2))/3;
v61=(a1(3)+c1(3)+e1(3))/3
v71=(b1(4)+d1(3)+f1(3))/3;
v81=(a1(4)+c1(4)+e1(4))/3;
v91=(b1(5)+d1(4)+f1(4))/3;
v101=(a1(5)+c1(5)+e1(5))/3;
v111=(b1(6)+d1(5)+f1(5))/3;
v121=(a1(6)+c1(6)+e1(6))/3;
131=b1(7);

v12=b2(1);
v22=(a2(1)+c2(1)+e2(1))/3;
v32=(b2(2)+d2(1)+f2(1))/3;
v42=(a2(2)+c2(2)+e2(2))/3;
v52=(b2(3)+d2(2)+f2(2))/3;
v62=(a2(3)+c2(3)+e2(3))/3;
v72=(b2(4)+d2(3)+f2(3))/3;
v82=(a2(4)+c2(4)+e2(4))/3;
v92=(b2(5)+d2(4)+f2(4))/3;
v102=(a2(5)+c2(5)+e2(5))/3;
v112=(b2(6)+d2(5)+f2(5))/3;
v122=(a2(6)+c2(6)+e2(6))/3;
v132=b2(7);

v14=b4(1);
v24=(a4(1)+c4(1)+e4(1))/3;
v34=(b4(2)+d4(1)+f4(1))/3;
v44=(a4(2)+c4(2)+e4(2))/3;
v54=(b4(3)+d4(2)+f4(2))/3;
v64=(a4(3)+c4(3)+e4(3))/3;
v74=(b4(4)+d4(3)+f4(3))/3;
v84=(a4(4)+c4(4)+e4(4))/3;
v94=(b4(5)+d4(4)+f4(4))/3;
v104=(a4(5)+c4(5)+e4(5))/3;
v114=(b4(6)+d4(5)+f4(5))/3;
v124=(a4(6)+c4(6)+e4(6))/3;
v134=b4(7);

v18=b8(1);
v28=(a8(1)+c8(1)+e8(1))/3;
v38=(b8(2)+d8(1)+f8(1))/3;
```

```
v48=(a8(2)+c8(2)+e8(2))/3;
v58=(b8(3)+d8(2)+f8(2))/3;
v68=(a8(3)+c8(3)+e8(3))/3;
v78=(b8(4)+d8(3)+f8(3))/3;
v88=(a8(4)+c8(4)+e8(4))/3;
v98=(b8(5)+d8(4)+f8(4))/3;
v108=(a8(5)+c8(5)+e8(5))/3;
v118=(b8(6)+d8(5)+f8(5))/3;
v128=(a8(6)+c8(6)+e8(6))/3;
v138=b8(7);

v116=b16(1);
v216=(a16(1)+c16(1)+e16(1))/3;
v316=(b16(2)+d16(1)+f16(1))/3;
v416=(a16(2)+c16(2)+e16(2))/3;
v516=(b16(3)+d16(2)+f16(2))/3;
v616=(a16(3)+c16(3)+e16(3))/3;
v716=(b16(4)+d16(3)+f16(3))/3;
v816=(a16(4)+c16(4)+e16(4))/3;
v916=(b16(5)+d16(4)+f16(4))/3;
v1016=(a16(5)+c16(5)+e16(5))/3;
v1116=(b16(6)+d16(5)+f16(5))/3;
v1216=(a16(6)+c16(6)+e16(6))/3;
v1316=b16(7);

v13=b3(1);
v23=(a3(1)+c3(1)+e3(1))/3
v33=(b3(2)+d3(1)+f3(1))/3;
v43=(a3(2)+c3(2)+e3(2))/3;
v53=(b3(3)+d3(2)+f3(2))/3;
v63=(a3(3)+c3(3)+e3(3))/3;
v73=(b3(4)+d3(3)+f3(3))/3;
v83=(a3(4)+c3(4)+e3(4))/3;
v93=(b3(5)+d3(4)+f3(4))/3;
v103=(a3(5)+c3(5)+e3(5))/3;
v113=(b3(6)+d3(5)+f3(5))/3;
v123=(a3(6)+c3(6)+e3(6))/3;
v133=b3(7);

% assemble one attenuation matrix

unt=[v1125 v2125 v3125 v4125 v5125 v6125 v7125 v8125 v9125 v10125 v11125 v12125 v13125
v1250 v2250 v3250 v4250 v5250 v6250 v7250 v8250 v9250 v10250 v11250 v12250 v13250
v15 v25 v35 v45 v55 v65 v75 v85 v95 v105 v115 v125 v135
v11 v21 v31 v41 v51 v61 v71 v81 v91 v101 v111 v121 v131
v12 v22 v32 v42 v52 v62 v72 v82 v92 v102 v112 v122 v132
v14 v24 v34 v44 v54 v64 v74 v84 v94 v104 v114 v124 v134
v18 v28 v38 v48 v58 v68 v78 v88 v98 v108 v118 v128 v138]
%v116 v216 v316 v416 v516 v616 v716 v816 v916 v1016 v1116 v1216 v1316
%v13 v23 v33 v43 v53 v63 v73 v83 v93 v103 v113 v123 v133];
```

```
%
%treated results half damped
%

a125=[-12.8 -12.9 -11.9 -17.1 -13.4 -9.2];
a250=[-6.1 -9 -10 -14.4 -14 -9.9];
a5=[1.4 -0.9 -0.1 -3.8 -5.8 -8.1];
a1=[3.4 0.3 3 1.5 -4.7 -6.7 ];
a2=[4.7 2.3 -1.9 -4.1 -8.6 -6.8 ];
a4=[5.1 -0.5 -6.3 -7.8 -13.4 -12];
a8=[7.2 -2.7 -8.8 -10.4 -16.8 -15.5];
a16=[];
a3=[];

b125=[-8.4 -9.4 -12.7 -10.8 -16.7 -8.1 -6.6];
b250=[-5.1 -7.5 -11.7 -10.5 -13.3 -15.9 -6.9];
b5=[6.5 -4.8 0.7 -2.7 -4.7 -7.7 -1.2];
b1=[11.2 3.7 3.5 -0.3 -1.2 -0.7 -0.7];
b2=[14.9 6.2 2.9 -0.5 -1.7 -2.4 -4.8];
b4=[16 2.8 -1.4 -6.3 -8.5 -10 -13.5];
b8=[18.3 7.6 -7.6 -10.4 -16.1 -19.2 -23.5];
b16=[];
b3=[];

c125=[-7.2 -13 -12.6 -14.4 -14.5 -7.5];
c250=[-3.8 -9 -9.4 -13.2 -14.7 -8.3];
c5=[2.3 -0.7 -1.4 -3.6 -7.3 -6.6];
c1=[2.7 1.2 2.5 -0.9 -4.8 -5.5];
c2=[5.3 2.5 -0.7 -7.1 -6.1 -8.8];
c4=[5.8 0.7 -4 -10.5 -9.4 -14.4];
c8=[7.2 -3.4 -7.5 -13.1 -14.3 -16.8];
c16=[];
c3=[];

d125=[-15.1 -11.9 -10.7 -16.3 -14.6];
d250=[-9.4 -11 -13.8 -15.3 -11.9];
d5=[2.4 -0.8 -7.6 -6.3 -8.6];
d1=[2 4.7 -2.1 -2.7 -2.6 ];
d2=[3.3 2.6 -5.2 -6 -7.2];
d4=[1.1 -4.5 -9.3 -11.6 -12.7];
d8=[-1.9 -9 -12.7 -15.8 -18.4];
d16=[];
d3=[];

e125=[-9.6 -11.2 -11.6 -14.4 -13 -11.2];
e250=[-6.7 -10.5 -11.2 -14.4 -14.7 -7.6];
e5=[4.1 -0.6 -5.6 -6 -5 -6.6];
e1=[7.5 5 3.6 -0.5 -2.2 -2.5];
e2=[7.1 3.5 2.9 -2.2 -5.8 -4.4];
e4=[3.8 -1.3 -3.6 -9.7 -13.1 -13.6];
e8=[6.9 -5.1 -12.6 -17.9 -22 -21.8]
```

```
e16=[];
e3=[];

f125=[-10.5 -10 -10.6 -15.5 -13.8];
f250=[-10.2 -12.5 -13.6 -15.7 -13.6];
f5=[1.8 -1.7 -5.4 -7.4 -9.3];
f1=[3.3 3 -0.9 -4.6 -3.5 ];
f2=[2.8 -1 -4.1 -7.7 -7.2];
f4=[0.5 -6.7 -9.3 -13.9 -13.3];
f8=[-2.4 -12 -13.8 -16.4 -19.5];
f16=[];
f3=[];

% average three joints per section (excluding end joints b1, b13)
%already written above

% assemble one attenuation matrix

tr1=[v1125 v2125 v3125 v4125 v5125 v6125 v7125 v8125 v9125 v10125 v11125 v12125 v13125
v1250 v2250 v3250 v4250 v5250 v6250 v7250 v8250 v9250 v10250 v11250 v12250 v13250
v15 v25 v35 v45 v55 v65 v75 v85 v95 v105 v115 v125 v135
v11 v21 v31 v41 v51 v61 v71 v81 v91 v101 v111 v121 v131
v12 v22 v32 v42 v52 v62 v72 v82 v92 v102 v112 v122 v132
v14 v24 v34 v44 v54 v64 v74 v84 v94 v104 v114 v124 v134
v18 v28 v38 v48 v58 v68 v78 v88 v98 v108 v118 v128 v138];


%Difference program
%
%
% set up the dimensions and frequencies
% f      -frequency octave band
% N      -section number
% x      -axial distance along truss (global)
% z      -strut length

f=[125 250 500 1000 2000 4000 8000 16000 32000]';
N=[1 2 3 4 5 6 7 8 9 10 11 12 13];
x=(N-1)*0.3843;
dif=tr1-unt
% normalize by the first section
b=zeros(7,13);
for j=1:13,
 b(1:7,j)=dif(1:7,1);
end
am=-1*(dif-b);

% plot of experimental differential attenuation curves, 2 graphs
firstone=0;
if firstone==1,
 plot(x,am(1,1:13),'-',x,am(2,1:13),'--',x,am(3,1:13),'-.',x,am(4,1:13),':')  axis([0 5 -5 40])
```

```
 %gtext('Average of all Joints at Each Section')
 %  LEGEND WORKS FOR MATLAB 4.1 ONLY (ATHENA)
 legend('125 Hz octave','250 Hz octave','500 Hz octave','1 kHz octave')
 %gtext('__ 125 Hz octave')
 %gtext('-- 250 kHz octave')
 %gtext('-. 500 Hz octave')
 %gtext('.. 1 kHz octave')
end

secdone=1;
if secdone==1,
 plot(x,am(5,1:13),'-',x,am(6,1:13),'--',x,am(7,1:13),'-.')
 axis([0 5 0 40])
% gtext('Average of all Joints at Each Section')
 legend('2 kHz octave','4 kHz octave','8 kHz octave')
% gtext('__ 2 kHz octave')
% gtext('-- 4 kHz octave')
% gtext('-. 8 kHz octave')
% gtext('.. 16 kHz octave'
% gtext('*  32 kHz octave')

end

xlabel('Axial Distance Along Truss (m)')
ylabel('Attenuation (dB) ')
%title('Attenuation of Acceleration vs. Distance From Force Excitation')
```

Figures 4.7 and 4.8: Difference of attenuation versus axial distance between the fully damped and the undamped configuration
(same program, I only mention the experimental values)

```
a125=[-6.3 -14.6 -11.9 -16.9 -10.4 -8.8];
a250=[-5.4 -9.2 -10.4 -16.8 -13.7  -9.7];
a5=[3.1 1.1 -0.2 -7.1 -4.8 -6.7];
a1=[4.9 2.2 2.1 -2.9 -3.7 -4.7];
a2=[5.6 0.3 -2.7 -10.2 -8.6 -9.8];
a4=[6 -1.4 -7.3 -14.3 -14.7 -15.9];
a8=[8.2 -3.5 -10.3 -14.2 -14.3 -15.7];

b125=[-3.5 -14.2 -14.8 -15.8 -14.8 -9.3 -8.5];
b250=[-3.2 -6.7 -11.9 -12.6 -12.5 -15.7 -8.4];
b5=[5.1 0.8 0.9 -3.1 -3.6 -9.6 -1.9];
b1=[10.6 4.2 2.9 -2.6 -1.5 -4.0 -2.1];
b2=[14 7.3 3.5 -2.9 -5.1 -5.9 -11.1];
b4=[15.3 4.5 2.1 -8.1 -8.7 -11.8 -18];
b8=[17.4 8.8 -3.9 -13.1 -11.8 -16.3 -25.7];

c125=[-12.1 -12.1 -11.7 -12.9 -14.2 -8];
c250=[-4.2 -8.9 -9.2 -12 -14.8 -9.2];
c5=[1.5 0.2 1.4 -5.3 -6.9 -6.2];
c1=[4.8 3.5 2.3 -0.7 -4.4 -4.7];
c2=[6.4 1.9 -0.6 -10.1 -9.9 -10.6];
c4=[6.7 1 -5.1 -8.9 -12.9 -14.3];
c8=[7.3 -2.5 -8.9 -9.8 -14 -16.8];

d125=[-10.4 -10.7 -7.2 -13.3 -11.6];
d250=[-5.5 -8.9 -11.4 -18.1 -11.5];
d5=[2.9 0 -8.9 -5.3 -8.8];
d1=[2.6 3.7 -4.5 -5.2 -7.0];
d2=[1.7 -1.4 -8.4 -9.6 -10.7];
d4=[0 -5.7 -11.3 -13.6 -15.8];
d8=[-2.2 -10.8 -15.3 -16.4 -18.6];

e125=[-9.6 -12.7 -14.7 -12.9 -15.6 -10.8];
e250=[-4.9 -12.5 -13.6 -15.5 -20.2 -7.6];
e5=[5.3 0.5 -5 -7.4 -5.4 -3.8];
e1=[8.8 5.7 3.5 -3.7 -5.7 -4.2];
e2=[8.1 3.8 2.6 -6.8 -8.7 -10];
e4=[7.8 -0.3 -3.8 -13.2 -13.9 -16.4];
e8=[8.8 -2.9 -11.2 -19.5 -17.6 -21.8];

f125=[-8.6 -14.2 -15.4 -14.1 -13.7];
f250=[-4.6 -16.7 -14.6 -13.8 -12.4];
f5=[2.5 -2.3 -8.5 -6 -8.6];
f1=[4.9 2.7 -4.7 -5.9 -7.0];
f2=[3.5 -0.5 -8.3 -11.4 -12];
f4=[0.8 -4.1 -12.9 -14.2 -15.4];
f8=[-1.3 -11.7 -17 -19.9 -21];
```

Figures 4.9: Difference of attenuation versus axial distance between the half damped and the undamped configuration

(same program, I only mention the experimental values)

```
a3=[3.3 0.6 -7.9 -8.6 -5.7 -7.1];
a5=[0.6 -8.3 1.5 -7.9 -7.1 -15];
a6=[7.4 -3.9 3.2 -0.9 -6.3 -8.9];
a7=[1.1 1.5 4.5 -0.4 -3.7 -6.3];

b3=[3.4 0.1 -2.3 -7 -6.7 -11.3 0.5];
b5=[5.8 -4.5 1.4 -2.8 -3.7 -7.2 -3.4];
b6=[11.1 -2 4.7 1.8 -1.7 -5.2 -2.4];
b7=[13.2 1.8 2.7 3.3 -2.1 -5 -6.2];

c3=[1.3 2.2 -1.9 -8.5 -6.7 -5.9];
c5=[-4.1 -3.3 5.8 -5.4 -10.2 -10.5];
c6=[2.9 1.8 6.4 0.7 -5.2 -6.9];
c7=[0 1.7 5.8 2 -6.5 -6.6];

d3=[-0.7 -2.3 -8.5 -6.1 -12.2 ];
d5=[3.4 1.2 -8.9 -10.1 -12];
d6=[-7.4 -1.3 -6.8 -6.3 1.6];
d7=[6.9 7.4 -4 -3.4 -3.6 ];

e3=[0.9 -2.3 -6.6 -6.7 -7.2 -3.8];
e5=[8.1 2 -8 -15.6 -2.1 -3.6];
e6=[9.4 0.7 -10.6 -1.9 -2.5 -0.9];
e7=[8.6 7.4 -1.2 -2.7 -6.8 -4.9];
e1=[8.8 5.7 3.5 -3.7 -5.7 -4.2];

f3=[-0.6 -5.2 -7 -4.3 -13.5];
f5=[1.2 0.6 -6.2 -8.4 -7.1];
f6=[6.5 -2.7 -6.3 -10.1 -0.1];
f7=[5.8 5.2 -4.2 -5.2 -4.5];
```

Fig 5.3: Attenuation versus frequency of flexural, longitudinal and torsional waves after 65 cm of treated rod and corresponding averaged values on octave bands

```
clear
clf
%plot flexural attenuation on a rod due to a continuous distribution of abs.
%
nu=0.19;
beta=2.8;
f=50:10:3000;
w=2.*pi.*f;
y=450./f;
kf=sqrt(w./(0.004*5096))
kif=kf.*imag((1+beta*(nu+i.*y.*y)./(nu+i.*y.*y-i)).^(0.25));
Af=8.686*kif*0.65;
%
%plot longitudinal attenuation
%
nu=0.34;
x=f./450;
kl=w./5091;
kil=kl.*imag((1+beta.*(1-i.*nu.*x)./(1-i.*nu.*x-x.*x)).^(0.5));
Al=8.69*kil*0.65;
%
%plot rotational attenuation
%
nu=0.34;
x=f./330;
kr=w./3000;
kil=kr.*imag((1+beta.*(1-i.*nu.*x)./(1-i.*nu.*x-x.*x)).^(0.5));
Ar=8.69*kil*0.65;
%
%legend('flexural waves','longitudinal waves','torsional waves');

%       average over octave bands

f0 = [125 250 500 1000 2000];
fl = f0./sqrt(2);
fu = sqrt(2)*f0;
nfl = round((fl-50)/10.0);
nfu = round((fu-50)/10.0);
for ii = 1:5,
        avgf(ii) = sum(Af(1,nfl(ii):nfu(ii)))/(nfu(ii)-nfl(ii)+1);
        avgl(ii) = sum(Al(1,nfl(ii):nfu(ii)))/(nfu(ii)-nfl(ii)+1);
        avgr(ii) = sum(Ar(1,nfl(ii):nfu(ii)))/(nfu(ii)-nfl(ii)+1);
end
%
axes('position',[0.1,0.1,0.65,0.65]);
plot(f,Af,'-',f,Al,'--',f,Ar,':',f0,avgf,'*',f0,avgl,'x',f0,avgr,'+');
legend('flexural waves','longitudinal waves','torsional waves');
```

Figures 5.8, 5.9, 5.10 and 5.11: Flexural attenuation for a finite beam at 500 Hz, 1000 Hz, 2000 Hz and 200 Hz

```
nu=0.19;
beta=2.9;
L=0.5;
f=500;
% f can also be equal to 1000, 2000 or 200
w=2.*pi.*f;
y=450./f;
kf=sqrt(w./(0.004*5096))
k=kf.*(1+beta*(nu+i.*y.*y)./(nu+i.*y.*y-i)).^(0.25);
x=0:0.001:L;
A=-10*log(exp(-imag(k).*x));
g=(1./(exp(-i.*k.*L)-exp(i.*k.*L))).*(exp(i.*k.*(x-L))+exp(i.*k.*L).*exp(-i.*k.*x));
magg=(real(g).^2+imag(g).^2).^(0.5);
magG=-10.*log(magg);
axes('position',[0.2,0.2,0.56,0.56]);
plot(x,magG,'-',x,A,'--');
 legend('finite beam','semi-infinite beam')

ylabel('Attenuation (dB) ')
```

Figures 5.14, 5.15 and 5.16: Analytical predictions for the transfer functions

```
clear
clf
nu=0.19;
beta=3;
L=0.5;
f=100:10:2100;
w=2.*pi.*f;
y=500./f;
kf=sqrt(w./(0.004*5096))
k=kf.*(1+beta*(nu+i.*y.*y)./(nu+i.*y.*y-i)).^(0.25);
%
%calculation at X=0.03
%
x=0.03;
A0=10*log(exp(-imag(k).*x));
g0=(1./(exp(-i.*k.*L)-exp(i.*k.*L))).*(exp(i.*k.*(x-L))+exp(i.*k.*L).*exp(-i.*k.*x));
magg0=(real(g0).^2+imag(g0).^2).^(0.5);
magG0=10.*log(magg0);
%
%Calculation at X=0.3
% the calculation is also done at X=0.1 and X=0.5
%
x=0.3;
AL=10*log(exp(-imag(k).*x));
```

```
gL=(1./(exp(-i.*k.*L)-exp(i.*k.*L))).*(exp(i.*k.*(x-L))+exp(i.*k.*L).*exp(-i.*k.*x));
maggL=(real(gL).^2+imag(gL).^2).^(0.5);
magGL=10.*log(maggL);
A=AL-A0;
magG=magGL-magG0;
axes('position',[0,0.1,1.0287,0.42]);
plot(f,magG,'-',f,A,'--');
axis([100 2100 -60 20]);
% legend('finite beam','semi-infinite beam')
```